MECHANICS OF AXONAL FORCE GENERATION IN EMBRYONIC *DROSOPHILA* NEURONS IN VIVO

BY
ALIREZA TOFANGCHI

DISSERTATION

Submitted in partial fulfillment of the requirements
for the degree of Doctor of Philosophy in Mechanical Engineering
in the Graduate College of the
University of Illinois at Urbana-Champaign, 2015

Urbana, Illinois

Doctoral Committee:

Professor Taher A. Saif, Chair and Director of Research
Professor Rhanor Gillette
Professor Iwona Jasiuk
Assistant Professor Mariana Elizabeth Kersh

Abstract

Neurons are excitable cell types that process and convey information by producing electrochemical signals. Neurons are known to be the core functional components of the brain and spinal cords in all animals. They communicate with other neuron or muscle junctions at specific points by releasing neurotransmitter at their synapses.

In recent years it has become increasingly evident that mechanical stimuli play an important role in the differentiation, growth, development, and motility of cells. Neurons in particular have been shown to be highly sensitive to a variety of mechanical inputs. For example, it has been shown that neurites undergo normal elongation when towed with an appropriately paced motor. Other evidences demonstrated that axonal elongation (up to several centimeters) can be induced by mechanical tension, and these axons retain their electrophysiological functions. More interestingly, recent experiments have provided new evidence of the role of mechanical forces in the functioning of neurons in vivo. These experiments have revealed that vesicle clustering in the presynaptic terminal of the neuromuscular junction in *Drosophila* embryos is dependent on mechanical tension in the axons. Vesicle clustering disappears with loss of mechanical tension and is regained upon restoration of tension. In addition, an increase in tension appears to increase the vesicle density at the synapse, suggesting that mechanical tension could be a signal to modulate synaptic plasticity in vivo.

Based on these in vitro and in vivo observations, it is hypothesized that if mechanical tension modulates synaptic plasticity, neurons are expected to respond to stimuli that alter the tension in their axons. To verify whether this is the case, the mechanical behavior of axons in live *Drosophila* embryos was examined. In this dissertation I addressed these questions: 1) Do *Drosophila* axons have a rest tension, and, if so, what is its magnitude? 2) Do *Drosophila* neurons actively regulate their tension when subjected to mechanical perturbation? 3) How do axons respond upon sustained loss of tension? And finally 4) what is the origin/ mechanism of force generation in axons at cytoskeletal and molecular level?

Our experiments showed that *Drosophila* neurons maintained a rest tension (1–13 nN) and behaved like viscoelastic solids in response to sustained stretching. More importantly, when the tension was suddenly diminished by a release of the externally applied force, the neurons contracted and actively generated force to restore tension, sometimes to a value close to their rest tension. In other set of experiments, mechanical tension in axonal shaft was removed by slackening the axons: bringing the neuro muscular junction (NMJ) towards the central nervous system (CNS) multiple times. It was observed that, in the absence of any pharmaceutical drug, axons always shortened and restored the straight configuration each time within 2-4 minutes. The total shortening was about 40% of the original length. This recovery however was significantly hampered with the depletion of ATP, inhibition of myosin motors, and disruption of actin filaments, but not with the disruption of microtubules. These results suggest that the actomyosin-machinery is the major active element in axonal contraction while microtubules contribute passively and minimally.

Acknowledgement

I would like to sincerely express my thank to my advisor, Prof. Taher Saif, who constantly help me to keep this research moving forward with his insightful comments, unlimited perseverance and support. Further, I would like to thank my committee members, Prof. Rhanor Gillette, Prof. Iwona Jasiuk and Prof Mariana Elizabeth Kersh for their sincere support and useful comment to make this dissertation possible to be presented today.

I'd like to take advantage of this opportunity to sincerely pay tribute to my family for their generous support during tough times of war; in particular my late mother who has been true source of inspiration and kindness during my childhood; and, my elder brothers Mohammad Reza and Kazem who financially supported me for college. I am also obliged to express my ultimate gratitude to my grand spiritual mentor, cousin Mosatfa Torabi Navid, who remarkably trained me how to handle tough situations in the absence of my parents. I also would like to thank my high school teachers Mr. Habibi , Seifikar and Mehri for their constant encouragement and genuine insights.

Finally, I would like to sincerely thank all mentors, lab mate and collaborators who helped me during this research work: Dr. Rajagopalan.Jagannathan, Dr. Sivaguru, Mayandi, Prof Sweedler, Jonathan V, Dr. Rubakhin, Stanislav, Anthony Fan, Wylie Ahmed, Brian Williams, Samantha Knoll. My Thanks also goes to Sandeep Anand, Elhebeary, Mohamed M Rashad Ibrahim, Bruno Azeredo and Mohammad Yakut Ali.

To my mother Seddigheh

and

my brother Mohammad Reza

Table of Contents

Chapter 1

Introduction

In recent years it has become increasingly evident that mechanical stimuli play an important role in the differentiation, growth, development, and motility of cells. Cells sense and respond to cues from their mechanical microenvironment as well as externally applied mechanical stimuli. For example, the lineage of stem cells is altered by the stiffness of the substrate on which they are grown [1], locomotion of epithelial cells and fibroblasts is regulated by substrate stiffness [2], and cell growth and development are dependent on substrate compliance [3]. Neurons in particular have been shown to be highly sensitive to a variety of mechanical inputs. A number of topics that have shown of the highest impact on morphological, structural and functional behavior of neuron are reviewed here.

1.1 Probing the influence of mechanical tension in neurons in vitro

Several studies have shown that neurites actively respond to mechanical forces. For example, Bray [4] showed that neurites undergo apparently normal elongation when towed with an appropriately paced motor. More recently, Pfister et al. [5] demonstrated that axonal elongation (up to several centimeters) can be induced by mechanical tension, and these axons retain their electrophysiological functions [6]. The intimate link between tension and axonal elongation is underscored by the fact that the elongation rate of PC-12 neurites, chick sensory neurons, and chick forebrain neurons all follow a robust linear relationship with applied tension (Fig 1.1) [7, 8 and 9]. In addition, experiments have also shown that tension applied to the margins of neuronal cell bodies can initiate neurites that exhibit all the typical characteristics of spontaneously initiated (growth cone-mediated) neurites [4 and 8]. Based on these observations and the evidence that advancing growth cones pull on the neuronal cell body, Heidemann et al. [10] suggested that tension acts as a proximate stimulus and regulator of axonal elongation.

The prominent role of tension in neuronal function is further underscored by the observation that a sudden reduction/loss of tension results in retraction of previously stable neurites in vitro. For example, chick sensory neurons subjected to neurite slackening undergo retraction and recover their tension, in many cases to a level greater than the initial value, within a period of 60–90 min [7]. Similar behavior is also seen in chick forebrain neurites, but to a much lesser degree [9]. Based on these observations, it has been suggested that a similar mechanism may underlie the retraction of axons from neuromuscular junctions [11,12,13], which results in a pattern of innervation in which only one motor neuron synapses with each skeletal muscle fiber. In fact, experiments have provided evidence that branches of developing axons that experience a buildup of mechanical tension stabilize and, in the process, cause the retraction of other branches and axon collaterals [14]. Of interest, application of mechanical forces above a threshold on the growth cone has also been shown to cause neurite retraction in a Ca^{+2}-dependent manner [15].

1.2 Probing the influence of mechanical tension in neurons *in vivo*

As outlined above, numerous studies have revealed the important role of mechanical tension in the initiation, development, elongation, and retraction of neurites in vitro. A similar role has been long suggested for mechanical forces in vivo. Weiss [16] first suggested that the final phase of elongation in peripheral neurons after the axon synapses with its target is mediated by the tension applied by the moving target. Van Essen [17] hypothesized that tension in axons may underlie many aspects of morphogenesis of the brain, especially the cortical regions of the brain. For example, he suggested that the folding of the cerebral cortex is due to the tension exerted by axons that connect relatively distant regions of the brain, and that the folding minimizes the communication time between interconnected brain regions. Unfortunately, many of these hypotheses remain unverified because studies detailing the in vivo mechanical behavior of neurons have been rather limited.

1.3 How mechanical tension alter the neuronal function?

Fatt and Katz argued that applying mechanical stretch on a muscle (and hence its embedded neurons) by 10–15% above its rest length initiated caused an escalation of 2.5–3 times in the rate of impulsive electrical potentials at the muscle endplate [18]. Another research performed by

Chen and Grinnell revealed that stretching a the entire frog muscle could at least double the release of neurotransmitters on their motor nerve [19]. They also demonstrated that integrin molecules mediate enhancement of neurotransmitter release.

Some recent experiments [20] have provided new evidence of the role of mechanical forces in the functioning of neurons in vivo. These experiments have shown that vesicle clustering in the presynaptic terminal of the neuromuscular junction in *Drosophila* embryos is dependent on mechanical tension in the axons. Vesicle clustering disappears with loss of mechanical tension and is regained upon restoration of tension. In addition, an increase in tension appears to increase the vesicle density at the synapse, suggesting that mechanical tension could be a signal to modulate synaptic plasticity in vivo (Fig 1.2).

In other attempts to study the time evolution of stretch-induced vesicle accumulation in vivo Ahmed et al. stretched intact axons while observing by live imaging [21]. They observed that vesicle accumulation amplified by nearly 30% after 5 minutes of mechanical stretch, as depicted in Fig 1.3. This stretch enhancement of vesicle accumulation last for at least 30 min after stretch was removed suggesting indicating a persistent change.

1.4 The overview of the current work

As outlined above, it is evident that mechanical inputs can majorly affect the structural and functional behavior of neurons both in vitro and in vivo. Now it is fair to raise a few key legitimate questions such as :

- If mechanical tension can modulates several neuronal behavior, do neurons are also expected to react to stimuli that perturb the tension in their axons?
- Do axons have a rest tension, and, if so, what is its magnitude?
- Do neurons actively regulate their tension when subjected to mechanical perturbation?
- How do axons respond upon sustained loss of tension? And finally,
- What is the origin/ mechanism of force generation in axons at cytoskeletal and molecular level?

In all parts of this dissertation, *Drosophila* embryo has been used as a biological model system for our experiments to address most key questions posed in the present work; in particular, those mechanistic cues that are presumably regulated by motor neurons *in vivo*.

I will discuss the details of the dissertation as following. First, a set of displacement-based high resolution micromechanical force sensors (MEMS) with a large force measurement range was designed and fabricated (Chapter 2). This device was then used to study the mechanical response of motor neurons in live *Drosophila* embryos (chapter 3). In the next step, efforts made to elucidate the key cytoskeletal components responsible for generating tension in axons (chapter 4). In the last attempt, the diametric regulation of single axon of *Drosophila* neurons subject to external stretch and control (free or intact) was investigated (chapter 5) . Finally, I conclude and present the outlook for the future work (chapter 6).

1.5 Figures

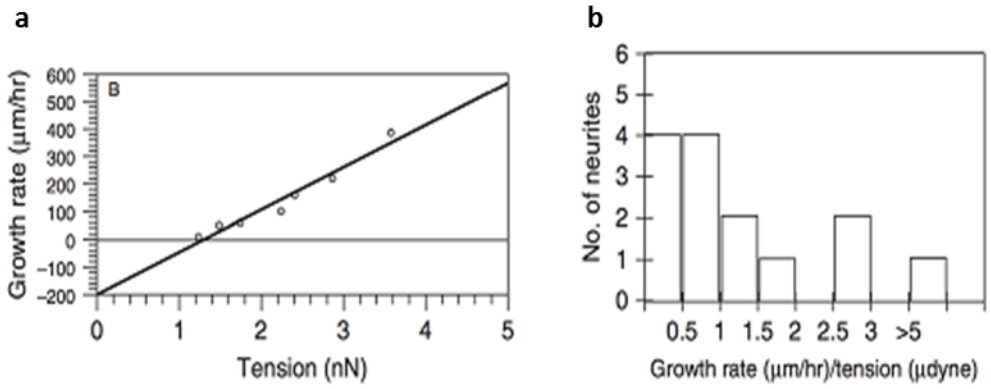

Figure 1.1: Eeffects of mechanical tension in neurons *in vitro*. (a) the degree of growth rate of a neurite varies as a function of induced tension. The zero-growth intercept demonstrates the tension threshold to prompt elongation. (b) Frequency distribution of tension sensitivity of neurite growth as a function of growth rate per unit tension, adapted from [7,8].

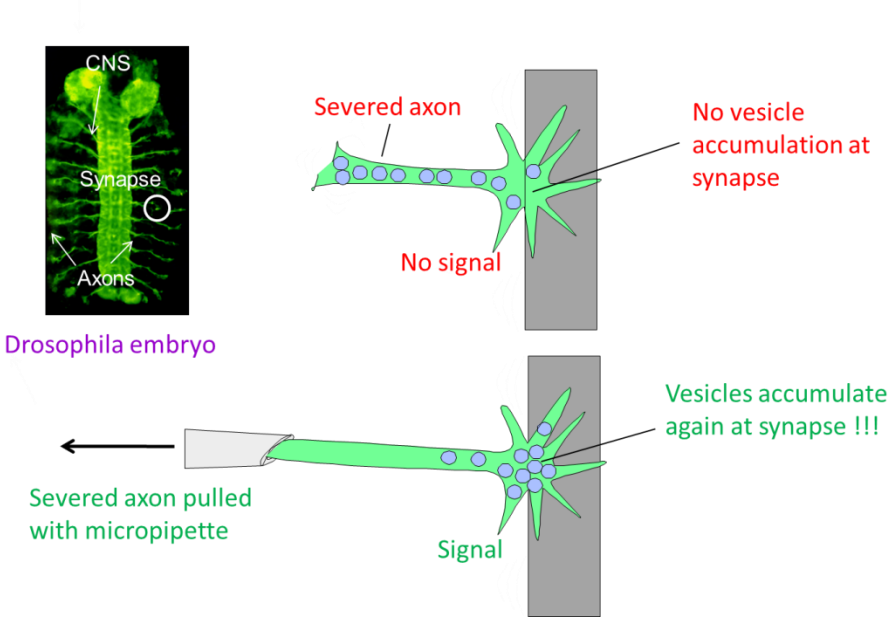

Figure 1.2: Axotomy Before synaptogenesis results in the loss of Presynaptic Vesicle Clustering. Mechanical Pull on Post-Synaptogenesis Severed Axon Restores Vesicle Clustering. Adapted from [20]

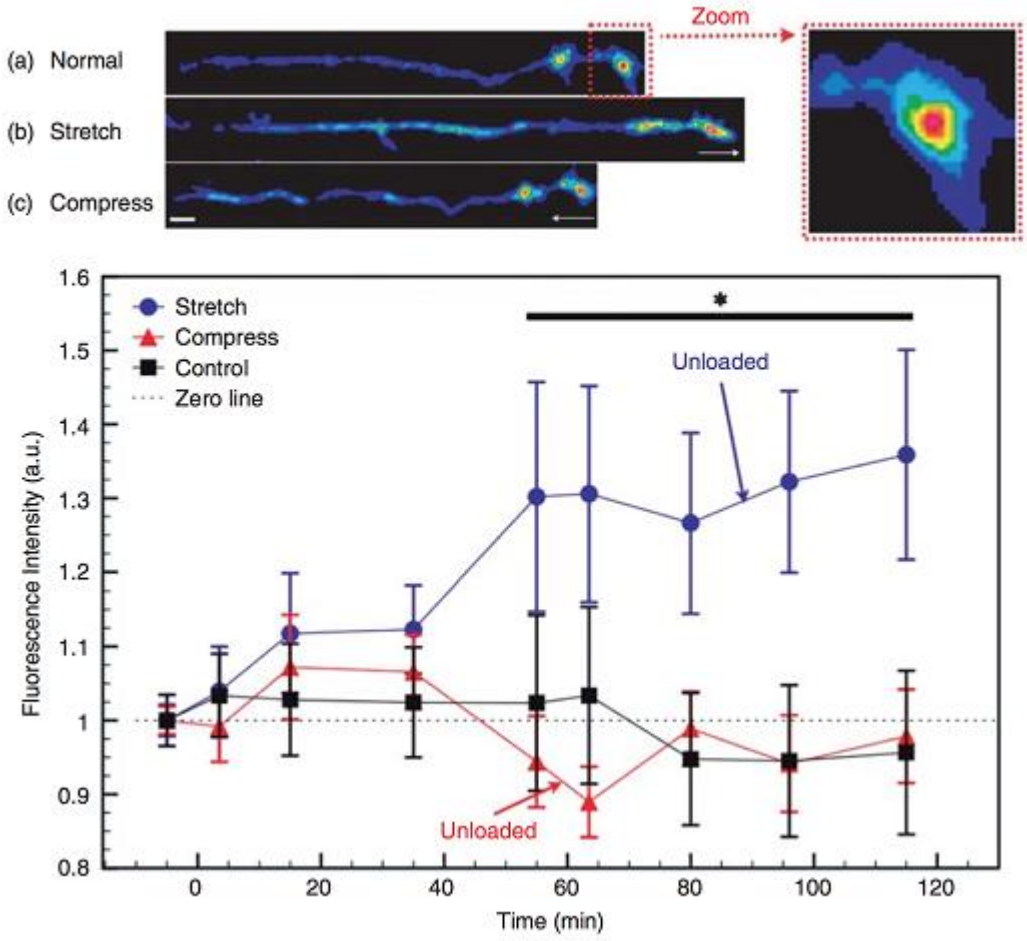

Figure 1.3: Stretch-induced accumulation of synaptic vesicles. (a) An intact axon is shown on the PDMS substrate. (b)The axon is stretched by pulling the substrate notice the tautness of the axon (c) The axon is by substrate compression notice the axon is squiggly (decreased tension) (scale bar= 5 mm). The graph depicts the fluorescence intensity of GFP-tagged vesicles at the presynaptic terminal *Drosophila NMJ* as a function of time. Control exhibit no major change in synaptic vesicle accumulation. Once axons are subjected to stretch, increased accumulation is occurred after 50 minutes and the effect remain for at least 30 min after relaxing the stress. In compressed axons, no major change observed in accumulation during compression or after it was released [21].

References

1.Engler, A. J., S. Sen, ., D. E. Discher. 2006. Matrix elasticity directs stem cell lineage specification. *Cell.* 126:677–689.

2. Pelham, Jr., R. J., and Y. Wang. 1997. Cell locomotion and focal adhesions are regulated by substrate flexibility. *Proc. Natl. Acad. Sci.* USA. 94:13661–13665.

3. Yeung, T., P. C. Georges, ., P. A. Janmey. 2005. Effects of substratestiffness on cell morphology, cytoskeletal structure, and adhesion. *Cell Motil. Cytoskeleton.* 60:24–34.

4. Bray, D. 1984. Axonal growth in response to experimentally applied mechanical tension. *Dev. Biol.* 102:379–389.

5. Pfister, B. J., A. Iwata, ., D. H. Smith. 2004. Extreme stretch growth of integrated axons. *J. Neurosci.* 24:7978–7983.

6. Pfister, B. J., D. P. Bonislawski, ., A. S. Cohen. 2006. Stretch-grown axons retain the ability to transmit active electrical signals. *FEBS Lett*. 580:3525–3531.

7. Dennerll, T. J., P. Lamoureux, R. E. Buxbaum, and S. R. Heidemann. 1989. The cytomechanics of axonal elongation and retraction. *J. Cell Biol.* 109:3073–3083.

8. Zheng, J., P. Lamoureux, ., S. R. Heidemann. 1991. Tensile regulation of axonal elongation and initiation. *J. Neurosci*. 11:1117–1125.

9. Chada, S., P. Lamoureux, ., S. R. Heidemann. 1997. Cytomechanics of neurite outgrowth from chick brain neurons. *J. Cell Sci*. 110: 1179–1186.

10. Heidemann, S. R., P. Lamoureux, and R. E. Buxbaum. 1995. Cytomechanics of axonal development. *Cell Biochem. Biophys*. 27:135–155.

11. Korneliussen, H., and J. K. S. Jansen. 1976. Morphological aspects ofthe elimination of polyneuronal innervation of skeletal muscle fibres in newborn rats. *J. Neurocytol*. 5:591–604.

12. Bixby, J. L. 1981. Ultrastructural observations on synapse elimination in neonatal rabbit skeletal muscle. *J. Neurocytol*. 10:81–100.

13. Morrison-Graham, K. 1983. An anatomical and electrophysiological study of synapse elimination at the developing frog neuromuscular junction. *Dev. Biol.* 99:298–311.

14. Anava, S., A. Greenbaum, ., A. Ayali. 2009. The regulative role of neurite mechanical tension in network development. *Biophys. J*. 96:1661–1670.

15. Franze, K., J. Gerdelmann, ., J. Ka ¨s. 2009. Neurite branch retraction is caused by a threshold-dependent mechanical impact. *Biophys.* J. 97:1883–1890.

16. Weiss, P. 1941. Nerve patterns: the mechanics of nerve growth. Growth. 5(SUPPL.):163–203.

17. Van Essen, D. C. 1997. A tension-based theory of morphogenesis and compact wiring in the central nervous system. *Nature*. 385:313–318.

18. Fatt, P & Katz, B. (1952) Spontaneous subthreshold activity at motor nerve endings. *The Journal of physiology* 117, 109–128.

19. Chen, B. M & Grinnell, A. D. (1995) Integrins and modulation of transmitter release from motor nerve terminals by stretch. *Science* 269, 1578–1580.

20. Siechen, S., S. Yang, ., T. Saif. 2009. Mechanical tension contributes to clustering of neurotransmitter vesicles at presynaptic terminals. Proc. Natl. Acad. Sci. USA. 106:12611–12616.

21. Ahmed, W. W, Li, T. C, Rubakhin, S. S, Chiba, A, Sweedler, J. V, & Saif, T. A. (2012) Mechanical tension modulates local and global vesicle dynamics in neurons. *Cellular and Molecular Bioengineering* 5,155–164.

Chapter 2

Design and Fabrication of a MEMS Force Sensor [1]

2.1 Motivation

In recent years, it has become increasingly evident that cell generated forces play an important role in many physiological process [1], [2]. Living cells respond to mechanical stimuli from their microenvironment both mechanically and biochemically [3]–[7]. Our understanding of how cells sense, apply, and respond to mechanical forces has been greatly aided by the development of a variety of new techniques [8]. These techniques fall broadly into two categories. The first class of techniques are used to study the mechanical behavior of entire cell populations, most commonly by imposing deformation through the substrate [9], [10] on which the cells are cultured. The second class of techniques are oriented toward studying the mechanical response of single cells and molecules. These include optical and magnetic tweezers [11], atomic force microscopes (AFMs) [12], optical stretchers [13], and magnetic twisting cytometry (MTC) [14]. Some techniques such as microfabricated post array detector [15] and embedded particle tracking [16] have been used for both single-cell and cell-population studies. In addition to the aforementioned techniques, several microelectromechanical systems (MEMS)- based techniques have been developed recently for biological force measurements, the examples of which include piezoresistive cantilevers [17] and MEMS capacitive sensors [18], [19].

Single-cell techniques such as MTC and optical tweezers often have high force and displacement resolution but can induce only small cell deformations (on the order of 1 μm) and measure small

1- Parts of this work have been published in " Rajagopalan, Jagannathan, Alireza Tofangchi, and M. Taher A. Saif. "Linear high-resolution biomems force sensors with large measurement range."*Microelectromechanical Systems, Journal of* 19.6 (2010): 1380-1389.

forces (10 nN or less). AFMs are also usually used to measure small forces, although much larger forces (in the millinewton range) can be measured by using stiff cantilevers but with a lower resolution. However, large cell deformations are physiologically relevant [20], [21], and to study cell response in such cases, a set of mechanical sensors based on microfabrication technologies was developed [22], [23]. These microfabricated sensors used flexible beams to sense forces up to 1 μN and used a simple displacement-based force-sensing method that precluded the need for complex electronics/optics. However, these force sensors had lower force resolution ($\approx$ 0.5 nN), and the force–displacement response was linear only over a limited displacement range ($<$ 50 μm). In this paper, we present a new class of micromechanical sensors that significantly mproves the resolution (50 pN) while preserving the range of force measurement of the aforementioned sensors. In addition, the new sensors have highly linear force–displacement response over the entire range of measurement and are fabricated using a simple two-mask process that ubstantially reduces the complexity of fabrication.

An essential requirement for micromechanical force sensors to be used in biological studies is the ability to operate in aqueous environments. This is a major challenge since the sensors have to withstand the extremely large forces required to break the meniscus during their immersion and removal from water. These capillary forces can cause severe structural damage to the sensors and compromise their functionality. To circumvent this problem, we have developed a novel scheme to insulate our force sensors from capillary forces during their immersion and removal from aqueous environments. We demonstrate the suitability of these sensors for biological applications by measuring the force-deformation response of axons in embryonic fruit flies (*Drosophila melanogaster*) *in vivo*.

2.2 Design of the force sensor

The force sensors are composed of a system of identical flexible beams attached to a rigid probe and a fixed beam that serves as a reference for displacement measurement [24] (Fig. 2.1). The principle of operation of the force sensor is as follows. When subjected to an external force, the beams deform, and their total deflection is found by optically measuring the relative displacement of the probe with respect to the fixed reference beam. The external force is then given by the total deflection of the beams multiplied by their combined stiffness. The combined stiffness of the

beams is calculated from their geometry and independently verified by calibration. Because of the use of optical measurement, only in-plane deflection of the beams can be measured in this setup. As evident from Fig. 2.1 , the beams are connected in series, and therefore, their combined stiffness is 1/*N* times the stiffness of each beam, where *N* is the total number of beams. As a result, the sensor can have high force resolution even if the stiffness of the individual beams is not very low. In addition, the resolution of the force sensors can be altered simply by varying *N* without changing the dimensions of the beams. More importantly, this design leads to a highly linear force–displacement relationship for the sensor. This is so because, even when the overall deflection (δ) is large, the deflection of the individual beams is still small, and hence, nonlinear effects are negligible.

We considered two different configurations of beams for our force sensors. In configuration I (Fig. 2.1 a), the basic repeating unit is a single flexible beam. The single beams are connected together by thick rigid beams to form a serpentine structure. In configuration II (Fig. 2.1 b), a pair of flexible beams is connected by a rigid beam to form a frame. The frames are then connected together by rigid beams to form a serpentine structure. In this configuration, the frames are the basic repeating units as opposed to single beams. The two configurations have different sensitivities to forces in different directions as shown in the following. Note that, in these sensors, only the *x* and *y* deflections of the probe are measured optically.

As discussed in [24] , we analyze the deflection of the probe in the *x*- and *y*-directions (δxp and δyp) and rotation φ when it is subjected to forces *Fx* and *Fy*. for both configurations.

Analysis for Configuration I:

Deflection due only Fx: $\delta_{xp} = \frac{NFxL^3}{12EI}$, $\delta_{yp} = 0$, $\varphi = 0$ (2.1)

Deflection due only Fy: $\delta_{xp} = 0$, $\delta_{yp} = \frac{F_y LN}{6EI}\left((2N^2 + 3N + 1)s^2 + (6N + 6)ds + 6d^2\right)$, (2.2)

$$\varphi = \frac{F_y L}{2EI}\left((N + 1)s + 2d\right)$$

Here, $I = \frac{bh^3}{12}$ and *E* is the Young's modulus. Our force sensors are made of single-crystal silicon, and the beams are oriented along the [110]-direction for which $E \approx 170$ GPa [25], [26]. *b*, *h*, and

L are the thickness, depth, and length of the beams, respectively. In these sensors, typically, *b* =2−4 μm, *h* = 10−40 μm, *L* = 2−3 mm, *d* = 0.3−0.4 mm,*s* = 32−34 μm, and *N* = 8−24 (see Fig. 2.2 for the definition of *s* and *d*).

Since *Fx* does not contribute to *δyp* and *Fy* does not contribute to *δxp*, the total *x* and *y* displacements of the probe are given by (2.1) and (2.2), respectively. In deriving these equations, we have assumed that the rotation *φi* of the beams is sufficiently small so that $\sin(\varphi) \approx \varphi$ and $\cos(\varphi) \approx 1$. This is a reasonably good approximation when $\varphi \leq 0.1$. Therefore ,from (2.2), we have

$$\varphi = \frac{F_y L}{2EI}\left((N+1)s + 2d\right) \leq 0.1 \qquad (2.3)$$

Taking *b* = 3 μm, *h* = 30 μm, *L* = 2 mm, *d* = 0.3 mm,*s* = 33 μm, and *N* = 20, we get *Fy* ≤ 38.4 nN. Therefore, the force–displacement relation for this configuration is linear only over a limited force range. For larger *Fy*, the force–displacement relationship becomes coupled (*Fy* contributes to *δxp*), as well as nonlinear. These nonlinearity and cross-coupling are avoided in configuration II as explained in the following. However, when both *Fx* and *Fy* are small, this configuration has some advantages. For example, the sensitivity of this configuration in the *x*-direction (*δxp/Fx*) and in the *y*-direction (*δyp/Fy*) is roughly similar, which is desirable when measuring both forces at the same time. To summarize, configuration I can measure forces in both *x*- and *y*-directions with high resolution but has a limited measurement range.

Analysis for Configuration II:

Deflection due only Fx: $\delta_{xp} = \frac{NFxL^3}{24EI}$, $\delta_{yp} = 0$, $\varphi = 0$ (2.4)

Deflection due only Fy $\delta_{xp} \approx 0$, $\delta_{yp} \approx 0$, $\varphi \approx 0$ (2.5)

As a result, the displacement of the probe (both *δxp* and *δyp*) due to *Fy* is negligible. On the other hand, this configuration is still highly sensitive to forces in the *x*-direction, and the relationship between *Fx* and *δxp* remains linear over a large force range(Fig. 2.7). Hence, this configuration ensures an uncoupled linear force–displacement response and is suitable for cases where only one force component is present or needed to be measured.

Out-of-plane deflection of the probe due to self – weight

In most MEMS devices, the effect of gravity is negligible because of their very small size. However, in these force sensors, the torsional stiffness of the beams is very low, and therefore, the rotation of the beams due to self-weight is significant. As a result, there is a fairly large deflection of the probe in the *z*-direction as shown in the following. The theoretical value of z-deflection was estimated in [24]. To verify these results, we calculated the out-of-plane deflection of this sensor due to self-weight by finite-element (FE) analysis (using ANSYS Multiphysics software). The deflection obtained from the FE analysis for this configuration is 14.12 μm (Fig.2.3), which is very close to the value obtained from the theoretical analysis.

Apart from the FE analysis, we also experimentally measured the out-of-plane deflection of three different force sensors. The difference between the theoretical prediction and experiments was less than 10% in all three cases. We further verified that the observed deflection is due to gravity and not due to residual stresses in the beams using a simple test. We measured the out-of-plane deflection first with the bottom side of the sensor facing downward and then the top side facing downward. In both cases, the deflection of the beams was downward (along the direction of gravity) and identical in magnitude. If residual stresses were responsible, the direction of the deflection would have reversed, or its magnitude would have been different in the two cases.

2.3 Fabrication process

The force sensors are fabricated using a simple two-mask process shown schematically in Fig. 2.4. In the first step, a 150-μm-thick (001)-oriented single-crystal silicon wafer is cleaned thoroughly, and a photoresist (AZ-5214) is spun on both sides of the wafer and patterned by photolithography. The top and bottom patterns are identical except that the bottom pattern does not have the force-sensing beams. Then, the wafer is etched from the bottom side using inductively coupled plasma deep reactive ion etching (ICP-DRIE) to the desired depth. The depth of etching controls the depth of the force-sensing beams in the sensor. For example, if the depth of etching is 120 μm, the depth of the beams is $150 - 120 = 30$ μm. After this, the photoresist on the bottom side of the wafer is removed by oxygen plasma, and a thin layer of aluminum (50 nm) issputter deposited on the bottom side. The wafer is then etched from the top side using ICP-DRIE until the aluminum layer is reached. It is during this step that the force-sensing beams and the other functional features of

the force sensor are created. The aluminum layer is deposited primarily for two purposes: 1) to prevent damage to the force-sensing beams during venting in the DRIE process and 2) to avoid damage to the beams from capillary forces when the force sensor is initially immersed into a liquid. In addition, the aluminum layer also facilitates heat transfer during the end of the DRIE step and prevents the structure from heating up [27], [28]. Otherwise, the etch can turn isotropic and destroy the vertical silicon sidewalls. In the last step, the photoresist on the top side is removed by oxygen plasma. Note that, at the end of the fabrication process, the force- sensing beams are still connected together by the aluminum layer.

Approaches for avoiding capillary forces

One of the main problems in MEMS is stiction, which is often encountered during the drying process after the release etch of freestanding components. The meniscus that develops when the wafer is removed from the liquid etchant brings the freestanding components into contact through capillary forces. Once in contact, the components remain stuck together even after the etchant dries out due to various adhesion forces. To avoid stiction-related failures, a number of approaches have been developed [29], [30]. Meniscus formation, for example, can be eliminated through drying techniques such as freeze sublimation or supercritical drying, but these techniques cannot prevent stiction that may occur during device operation. To prevent stiction during both the release etch and device operation, MEMS devices can be coated with antistiction coatings [31].

Capillary forces are also a major constraint in using micromechanical force sensors for biological applications. Since biological studies are usually performed in a liquid environment, the force sensors need to cross the air–liquid interface during their immersion and removal from liquids. Therefore, the force sensors must break the liquid meniscus irrespective of whether they are hydrophilic, hydrophobic, or hydroneutral. Since the force required to break the meniscus is usually very large [32], the force-sensing beams can be irreversibly damaged during this process. Even if the force sensors survive the immersion/removal process, they can suffer stiction-related failures. While antistiction coatings can mitigate stiction-related problems, they limit the scope of biological applications because the sensors often need to be functionalized with proteins such as fibronectin or laminin, and these proteins may not adhere to the antistiction coating. Therefore, to make our force sensors widely applicable for biological studies, we have established a simple scheme to avoid capillary forces.

First, the bottom side of the force sensor, with the aluminum film still intact (Fig. 2.5 a), is glued to a 150-μm-thick glass slide (approximately 7 mm wide and 1 cm long). The glass slide with the sensor is then immersed into a beaker containing a diluted solution of AZ 327 metal-ion-free (MIF) developer. During the immersion, the aluminum film protects the beams against damage from capillary forces. Once the sensor is immersed, the developer etches the aluminum film slowly, in the process releasing the flexible beams. In addition, the etching of the aluminum layer exposes the hydrophilic native silicon dioxide layer. Then, the developer is replaced with water by repeated dilution. When the glass slide is removed from the beaker, it retains a droplet of water, thereby keeping the sensor inundated in water, and therefore, the sensor does not experience any capillary forces.

2.4 Calibration process and verification

After the force-sensing beams were released, the sensorswere calibrated using a tungsten microneedle (N1) of known stiffness. Before calibrating the force sensors, the stiffness of microneedle N1 was obtained using a series of calibrations involving microneedles (N2–N4) with progressively higher stiffness. These tungsten microneedles had lengths ranging from 5 to 10 mm and diameters ranging from 14 to 40 μm. First, microneedle N1 was used to deform microneedle N2, and the ratio of their stiffness was obtained using force balance as

$$\frac{k_{N1}}{k_{N2}} = \frac{\delta_{N2}}{\delta_{N1}} = q_{12} \tag{2.6}$$

where kN1 and kN2 and δN1 and δN2 are the stiffness and deflection of needles N1 and N2, respectively. This procedure was then repeated to obtain the ratios (q23 and q34) of the stiffness of microneedles N2 and N3 and microneedles N3 and N4. As an example, the calibration of microneedle N3 with N4 is shown in Fig. 2.6a. The stiffness of microneedle N4(Fig. 2.6 b) was then directly obtained by hanging weights of known mass from the tip of the needle and measuring the tip displacement.

The stiffness of the force sensors was obtained by calibrating them with needle N1. From the force balance, $F = k\text{N1}\delta\text{N1} = k_{\text{sensor}}.\ \delta_{\text{sensor}}.\ k\text{N1}$ is known, and by measuring δN1 and δ_{sensor}, k_{sensor} can be calculated. The force–displacement relationship of two sensors in configuration II is shown in Fig. 2.7. The stiffness (kx) of the two sensors obtained from calibration is 0.427 and 4.135

nN/μm, respectively. The calibration also confirmed the linearity of the force response over a large ($\approx$ 150 μm) displacement range. Using image processing techniques (e.g., digital image correlation), one can measure displacements with an accuracy of about 100 nm from optical images. Therefore,the force resolution of the stiffer sensor is about 500 pN, andthe softer sensor is about 50 pN.

We also performed FE analysis of the in-plane deformation of a force sensor in configuration II. The dimensions of this sensor are exactly the same as the one in Fig. 2.3. The stiffness of the sensor along the *x*-direction (*kx*) is 0.34 nN/μm, whereas *ky* is 118 nN/μm ($\approx$ 350*kx*), showing that the sensor is sensitive only to *Fx*. The results also show that the force-deformation response remains linear even when *Fx* is 1 μN and δx is close to 3 mm. More importantly, the maximum stress in the beams is only 76 MPa (Fig. 2.8), which is about ten times lower than the failure strength of silicon even after accounting for processing-induced reductions in strength [24]. These results show that our sensors can measure forces ranging from tens of piconewtons to several hundred nanonewtons without failure while retaining linearity.

2.5 Figures

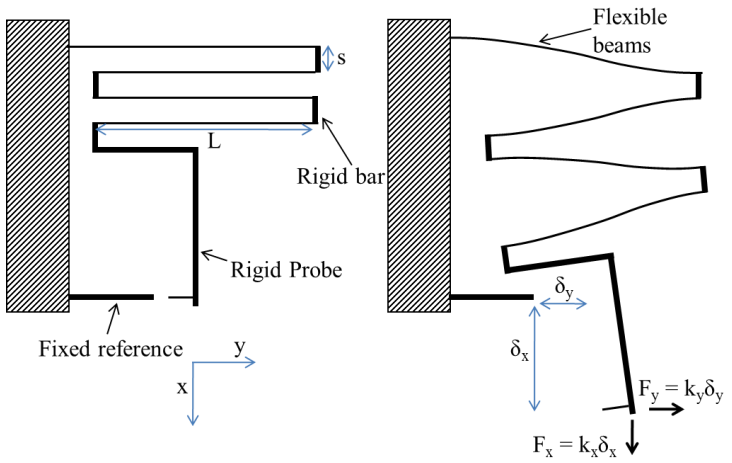

Fig. 2.1: Schematic of the force sensor. Because the flexible beams are connected in series, the deflection of the individual beams is small even when the overall deflection is large. This leads to high force resolution, as well as large linear force–displacement range.

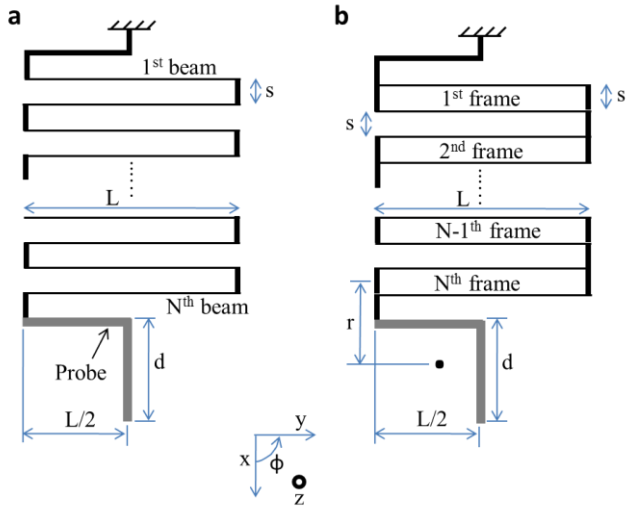

Fig. 2.2: Two configurations of beams considered for the force sensors. (a) Configuration I, where the basic repeating element is a single flexible beam. The probe is indicated in gray color. (b) Configuration II, where the repeating element is a frame. The black dot represents the center of mass of the probe. In both configurations, all the elements except the flexible beams are assumed to be rigid.

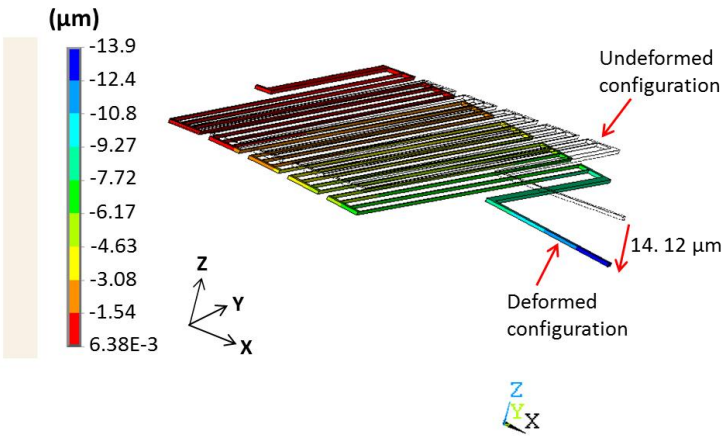

Fig. 2.3: Finite Element analysis of the out-of-plane deflection of a force sensor in configuration II due to self-weight. The dimensions of the sensor are given in the text. The deflection obtained from the FE analysis (14.12 μm) is very close to the value obtained from theory (14.32 μm). For easier visualization, the deflection of the sensor has been magnified ten times in the figure.

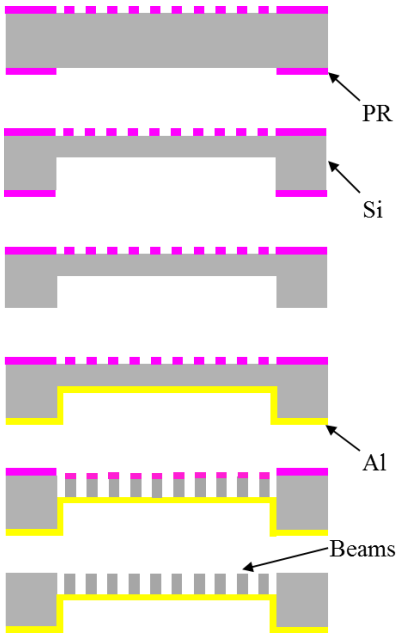

Fig. 2.4: Schematic of the fabrication process. Note that the beams are connected together by the aluminum film at the end of the process.

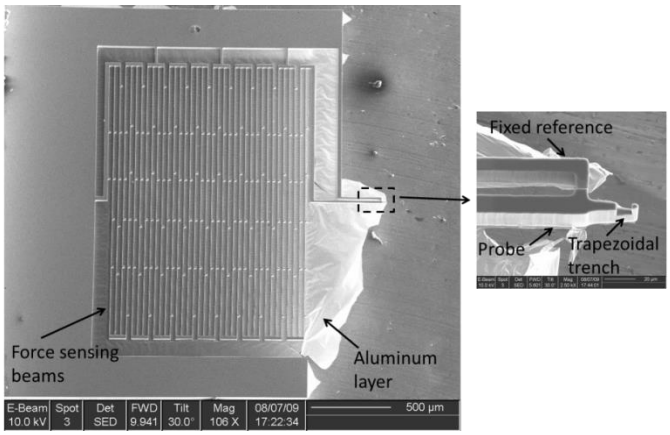

Fig. 2.5: (a) Scanning electron micrograph of a force sensor with the aluminum film still intact. (b) Magnified view of the probe and the reference beam. A trapezoidal trench was cut into the probe using focused ion beam milling to enable easier gripping of the axons

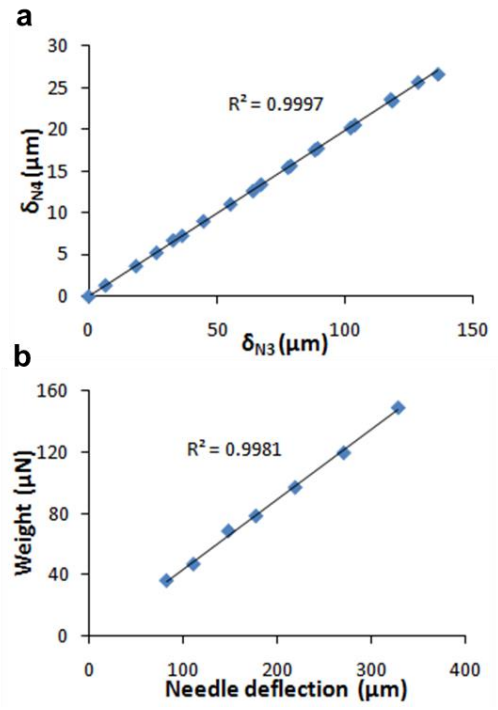

Fig. 2.6: (a) Calibration of microneedle N3 with needle N4. δN3 and δN4 are the deflections of needles N3 and N4, which are inversely proportional to their stiffness. q34 (kN3/kN4) is given by the slope of the line (0.1982 μm/μm). (b) Direct calibration of needle N4 using weights. The slope of the line (0.4491 μN/μm) gives the stiffness of needle N4.

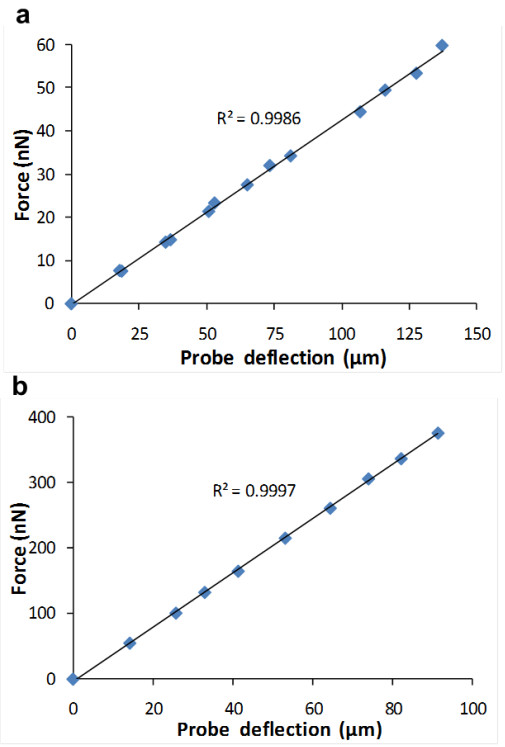

Fig. 2.7: Force–displacement (*Fx* versus δx) relation of two force sensors in configuration II obtained by calibration with microneedle N1. The stiffness of the two sensors is (a) 0.427 and (b) 4.135 nN/μm, respectively. The figure shows the linearity of the force response of the sensor over a large displacement range.

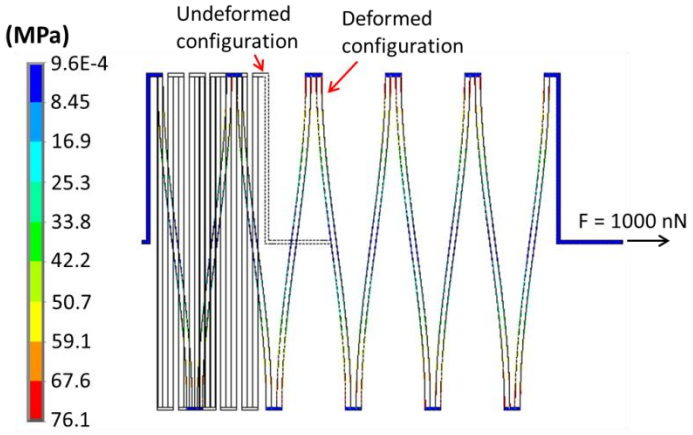

Fig. 2.8:. Stress distribution in the force sensor for *Fx* = 1 μN, obtained using FE analysis. The maximum stress at this high force is still only 76 MPa (see scale bar). The deformation of the sensor has been scaled down to 0.8 times the actual deformation in the figure.

References

1. G. Bao and S. Suresh, "Cell and molecular mechanics of biological materials," *Nat. Mater.*, vol. 2, no. 11, pp. 715–725, Nov. 2003.

2. D. Ingber, "Cellular mechanotransduction: Putting all the pieces togetheragain," *FASEB J.*, vol. 20, no. 7, pp. 811–827, May 2006.

3.N.Wang, J. Butler, and D. Ingber, "Mechanotransduction across the cell surface and through the cytoskeleton," *Science*, vol. 260, no. 5111,pp. 1124–1127, May 1993.

4. C. Chen, M. Mrksich, S. Huang, G. Whitesides, and D. Ingber, "Geometric control of cell life and death," *Science*, vol. 276, no. 5317, pp. 1425–1428, May 1997.

5. C. Galbraith and M. Sheetz, "A micromachined device provides a newbend on fibroblast traction forces," *Proc. Nat. Acad. Sci. USA*, vol. 94,no. 17, pp. 9114–9118, Aug. 1997.

6. S. Suresh, J. Spatz, J. Mills, A. Micoulet, M. Dao, C. Lim, M. Beil, and T. Seufferlein, "Connections between single-cell biomechanics and human disease states: Gastrointestinal cancer and malaria," *Acta Biomater.*, vol. 1, no. 1, pp. 15–30, Jan. 2005.

7. A. Engler, S. Sen, H. Sweeney, and D. Discher, "Matrix elasticity directs stem cell lineage specification," *Cell*, vol. 126, no. 4, pp. 677–689,Aug. 2006.8. K. J. Van Vliet, G. Bao, and S. Suresh, "The biomechanics toolbox: Experimental approaches for living cells and biomolecules," *Acta Mater.*, vol. 51, no. 19, pp. 5881–5905, Nov. 2003.

8. K. J. Van Vliet, G. Bao, and S. Suresh, "The biomechanics toolbox: Experimental approaches for living cells and biomolecules," Acta Mater., vol. 51, no. 19, pp. 5881–5905, Nov. 2003.

9. H. Wang, W. Ip, R. Boissy, and E. Grood, "Cell orientation response to cyclically deformed substrates: Experimental validation of a cell model," *J. Biomech.*, vol. 28, no. 12, pp. 1543–1552, Dec. 1995.

10. A. Lee, T. Delhaas, L. Waldman, D. Mackenna, F. Villarreal, and A. McCulloch, "An equibiaxial strain system for cultured cells," *Amer. J. Physiol. Cell. Physiol.*, vol. 271, no. 4, pp. C1 400–C1 408, Oct. 1996.

11. A. Bausch, W. Möller, and E. W. Sackmann, "Measurement of local viscoelasticity and forces in living cells by magnetic tweezers," *Biophys. J.*, vol. 76, no. 1, pp. 573–579, Jan. 1999.

12. M. Radmacher, "Measuring the elastic properties of living cells by the atomic force microscope," *Methods Cell Biol.*, vol. 68, pp. 67–90, 2002. 13. J. Guck, J. A. Chiang, and J. Kas, "The optical stretcher: A novel tool to characterize the cytoskeleton," *Mol. Biol. Cell*, vol. 9, p. 609, 1998.

13. J. Guck, J. A. Chiang, and J. Kas, "The optical stretcher: A novel tool to characterize the cytoskeleton," Mol. Biol. Cell, vol. 9, p. 609, 1998.

14. M. Puig-De-Morales, M. Grabulosa, J. Alcaraz, J. Mullol, G. Maksym, J. Fredberg, and D. Navajas, "Measurement of cell microrheology by magnetic twisting cytometry with frequency domain demodulation," *J. Appl. Physiol.*, vol. 91, no. 3, pp. 1152–1159, Sep. 2001.

15. J. Tan, J. Tien, D. Pirone, D. Gray, K. Bhadriraju, and C. Chen, "Cells lying on a bed of icroneedles: An approach to isolate mechanical force," *Proc. Nat. Acad. Sci. USA*, vol. 100, no. 4, pp. 1484–1489, Feb. 2003.

16. K. Beningo and Y.-L. Wang, "Flexible substrata for the detecton of cellular traction forces," *Trends Cell Biol.*, vol. 12, no. 2, pp. 79–84, Feb. 2002.

17. S.-J. Park, M. B. Goodman, and B. L. Pruitt, "Analysis of nematode mechanics by piezoresistive displacement clamp," *Proc. Nat. Acad. Sci. USA*, vol. 104, no. 44, pp. 17 376–17 381, Oct. 2007.

18. Y. Sun, K. T. Wan, K. P. Roberts, J. C. Bischof, and B. J. Nelson, "Mechanical property characterization of mouse zona pellucida," *IEEE Trans. Nanobiosci.*, vol. 2, no. 4, pp. 279–286, Dec. 2003.

19. K. Kim, J. Cheng, Q. Liu, X. Y. Wu, and Y. Sun, "Investigation of mechanical properties of soft hydrogel microcapsules in relation to protein delivery using a MEMS force sensor," *J. Biomed. Mater. Res.—Part A*, vol. 92, no. 1, pp. 103–113, Jan. 2010.

20. F. Silver, *Biological Materials: Structure, Mechanical Properties, and Modeling of Soft Tissues*. New York: New York Univ. Press, 1987.

21. B. Pfister, T. Weihs, M. Betenbaugh, and G. Bao, "An *in vitro* uniaxial stretch model for axonal injury," *Ann. Biomed. Eng.*, vol. 31, no. 5, pp. 589–598, May 2003.

22. S. Yang and T. Saif, "Micromachined force sensors for the study of cell mechanics," *Rev. Sci. Instrum.*, vol. 76, no. 4, pp. 1–8, Apr. 2005.

23. S. Yang and M. Saif, "MEMS based force sensors for the study of indentation response of single living cells," *Sens. Actuators A, Phys.*, vol. 135, no. 1, pp. 16–22, Mar. 2007.

24. Rajagopalan, Jagannathan, Alireza Tofangchi, and M. Taher A. Saif. "Linear high-resolution biomems force sensors with large measurement range."*Microelectromechanical Systems, Journal of* 19.6 (2010): 1380-1389.

25. T. Yi, L. Li, and C. J. Kim, "Microscale material testing of single crystalline silicon: Process effects on surface morphology and tensile strength," *Sens. Actuators A, Phys.*, vol. 83, no. 1–3, pp. 172–178, May 2000.

26 . T. Namazu, Y. Isono, and T. Tanaka, "Evaluation of size effect on mechanical properties of single crystal silicon by nanoscale bending test using AFM," *J. Microelectromech. Syst.*, vol. 9, no. 4, pp. 450–459, Dec. 2000.

27. S. E. Alper, A. Aydemir, and T. Akin, "Stepped-etching for preserving critical dimensions in through-wafer deep reactive ion etching of thick silicon," in *Proc. Int. Conf. Solid-State Sens., Actuators, Microsystem, Transducers*, Denver, CO, Jun. 2009, vol. 1110–1113.

28. P. J. Gilgunn and G. K. Fedder, "On the origin of selectivity and anisotropy loss during microstructure release etch," *J. Micromech. Microeng.*, vol. 20, no. 3, p. 035 021, Mar. 2010.

29. W. M. Van Spengen, "MEMS reliability from a failure mechanisms perspective," *Microelectron. Reliab.*, vol. 43, no. 7, pp. 1049–1060, Jul. 2003.

30. B. Bhushan, "Adhesion and stiction: Mechanisms, measurement techniques, and methods for reduction," *J. Vac. Sci. Technol. B, Microelectron. Nanometer Struct.*, vol. 21, no. 6, pp. 2262–2296, Nov. 2003.

31. B. H. Kim, T. D. Chung, C. H. Oh, and K. Chun, "A new organic modifier for anti-stiction," *J. Microelectromech. Syst.*, vol. 10, no. 1, pp. 33–40, Mar. 2001.

Chapter 3

Axonal Force Regulation in Drosophila Neurons in vivo[1]

3.1 Motivation

As it is evident in the previous research work that mechanical tension indeed modulates a number of neuronal behavior [1,2,3,4] , one would expect neurons to respond to stimuli that alter the tension in the axons. To verify whether this is the case, we examined the mechanical behavior of axons in live *Drosophila* embryos. In particular, we investigated two main questions:

a) Do *Drosophila* axons have a rest tension, and, if so, what is its magnitude?

b) Do *Drosophila* neurons regulate their tension when subjected to mechanical perturbation?

c) How do axons respond to loss of tension?

To answer these questions, we used high-resolution micromechanical force sensors, as described in chapter 2, to systematically deform the axons and measured their force response simultaneously. Our measurements revealed the following [7]:

1. Axons have a rest tension in the range of 1–13 nN.

2. In response to fast deformation, axons behave like elastic springs, showing a linear force-deformation response that is followed by force relaxation to a steady-state value after 15–30 min.

3. When the applied deformation is sufficiently large, the axons adopt a slack appearance upon removal of force. However, the axons tauten and build up tension, sometimes to a level close to their rest tension, within a period of 15–60 min.

1- Parts of this work have been published as Rajagopalan, Jagannathan, Alireza Tofangchi, and M. Taher A. Saif. "Drosophila neurons actively regulate axonal tension in vivo", *Biophysical journal* 99.10 (2010): 3208-3215.

Furthermore, our observations of neuronal mechanical behavior in vivo are remarkably similar to those made in previous in vitro studies, suggesting that mechanical forces could also prominently influence neuronal growth and function in vivo.

3.2 Materials and methods

Culture of *Drosophila* embryos. Transgenic *Drosophila* (elav′-GAL4/UAS-gap::GFP) expressing green fluorescent protein (GFP) in all neuronal membranes (Fig. 3.1) were used for the experiments. For embryo harvesting, the *Drosophila* were cultured on standard grape agar plates at ∼25°C. Embryonic dissection was carried out on glass coverslides as previously described by Budnik et al. [5]. Briefly, the embryos were dechorionated with a 50/50 bleach and water solution for 2 min and then rinsed with deionized water. Embryos of the correct age (16–18 h after egg laying) were placed on double-sided tape, flooded with insect saline solution, and then devitellinized before they were placed on the glass surface. The embryos were oriented such that the ventral nerve cord was closest to the glass surface, and a glass dissection needle was used to make a dorsal incision. The incision was made from posterior to anterior along the embryo to remove the guts and lay the body walls down flat. Then the axons of the aCC motor neuron and the RP2 motor neuron, which comprise the intersegmental nerve [6], were isolated by gently removing other nearby sensory and motor neurons as well as the fat cells and muscle fibers around them. The neuromuscular junctions (NMJs) of the aCC and RP2 neuron were not damaged during this process. After isolation, in some cases the axon of the RP2 neuron was excised near its NMJ, leaving only the axon of the aCC neuron intact. In most cases, both axons were intact and we measured their combined response. For dissection materials, glass slides were incubated with 10% 3-minopropyl triethoxysilane to improve embryo adhesion, and glass microneedles were created using a Sutter Instruments (Novota, CA) laser-based micropipette/fiber puller. For details see [7]

Deformation of axons and force measurement. The isolated axons of *Drosophila* neurons were deformed with the use of micromechanical force sensors and their force response was monitored simultaneously. All experiments were performed within 3 h after embryo dissection. The operation of force sensors has been described in detail elsewhere [8]. Briefly, the sensor consists of a rigid probe attached to a series of flexible beams. When a force is applied on the probe, the flexible beams deform in response to it. The deflection of the beams is measured by the

relative displacement of the probe with respect to a fixed reference. The force on the probe is then calculated by multiplying the stiffness of the beams with the measured deflection. Once the force on the probe is known, the tension in the axon is calculated using a simple force balance as shown in Fig. 3.2. The movement of the force sensors was controlled by means of an x-y-z piezo actuator (NanoPZ PZC200; Newport, Irvine, CA). Live imaging of the axon under the applied deformation was carried out on an inverted microscope (IX81; Olympus, Nashua, NH). The time-lapse images were analyzed using MATLAB (The MathWorks, Natick, MA) to measure the deformation and force on the individual axons. The length of the axons in the axon contraction experiments was measured using the NeuronJ plug-in of ImageJ software (U.S. National Institutes of Health, Bethesda, MD).

3.3 Results

We investigated the mechanical behavior of the axons by studying their response to systematic stretching experiments, which consisted of the following steps:

Step 1. The axons were loaded within a period of 1–2 min to a predetermined level of stretch (usually <50% of the axon length) using the force sensor.

Step 2. The force sensor was held fixed and the time evolution of axonal force was recorded over a period of 10–15 min.

Step 3.The force sensor was unloaded (within 2 min) to release the force on the axon.

These three steps together constitute one complete deformation cycle. The mechanical behavior of 14 axons, each from a different embryo, were examined in this manner. Twelve of the 14 axons were subjected to at least two deformation cycles.

Axon response is linear during loading. During fast loading (step 1), a linear relationship between axonal force and applied deformation was found in all the axons. In effect, the axons behaved like elastic springs when subjected to sudden changes in force. The stiffness of the axons, given by the slope of the force-deformation curve, varied from embryo to embryo with values ranging from 0.2 nN/μm to 1.2 nN/μm. In addition, individual axons also showed variation in stiffness from one cycle to the next. As discussed below, the stiffness of the axons appeared to have a direct correlation with the extent of force relaxation in the previous deformation cycle, with larger force relaxation leading to lower axonal stiffness in the subsequent cycle and vice versa. The response of two representative axons during the first loading is shown in Fig. 3.3. From our

visual observation, axons that were thicker usually seemed to have higher stiffness, but an attempt to correlate axonal diameter with stiffness was hindered by the presence of fat cells around the axons in some of the experiments.

To verify whether axons maintain a rest tension, we extrapolated the force-deformation curve of each axon during the first loading to zero deformation. The extrapolation yielded a positive force value for 13 out of 14 axons (Fig. 3.3*C*), confirming that the axons maintain a rest tension in vivo. In similarity to the stiffness values, there was a fairly large variation in the rest tensions of the axons, with values ranging from 1 nN to 13 nN. The presence of a rest tension, we note, is consistent with the taut appearance of the axons. By extrapolating the force-deformation curve to zero force, we found that the stretch in the axons in their resting state was ~5–15%.

Axon show force relaxation after loading. When the force sensor was held fixed after loading (step 2), the force in the axons decreased over time. An initial fast decay in force was followed by a more gradual decrease to a steady-state value over a period of 15–30 min in all the experiments. As illustrated in Fig. 3.2, when the axonal force is reduced, the length of the axon continuously increases. Fig. 3.4 shows the decay in force and the corresponding increase in length over time of the same axon shown in Fig. 3.3*A*. As is evident from Fig. 3.4, the axonal length can increase substantially during force relaxation. It should be noted that the increase in axon length for a given amount of force relaxation depends on the force sensor stiffness because of the coupling between the force sensor deflection and axonal length. For a given reduction in force, the increase in axon length is large when the force sensor stiffness is small, and vice versa. However, the extent of force relaxation in different axons, and consequently their increase in length, did not show any correlation with the stiffness of the force sensor used to measure their response.

As with the rest tension and stiffness, the axons also showed considerable variation in the extent of their force relaxation. The extent of force relaxation ((initial force - steady-state force)/initial force) ranged from 30% to nearly 90% (Fig. 3.5*A*). Of interest, the force relaxation in the axons had no correlation with either the initial force or the deformation imposed on the axons However, the extent of relaxation appeared to affect the stiffness of the axons in the subsequent loading. Axons that showed low relaxation typically exhibited higher stiffness during the next loading, whereas the opposite was true for axons that underwent large relaxation (Fig. 3.5*B*). The axons

that exhibited a large relaxation in force (>75%) noticeably thinned during the process, but the thinning was not uniform and was usually restricted to a particular region of the axon (Fig. 3.5*C*).

Axons contracts and build up tension after unloading. After unloading (step 3), the axons showed two types of behavior. In 12 of the 14 experiments the axons developed a slack appearance after the first unloading, i.e., they were free of tension. In the other two experiments the axons immediately regained their taut appearance upon unloading. In the 12 axons that became slack after unloading, the force sensor was held fixed and the response of the axons was recorded. All 12 axons reduced their length and visibly straightened over time. After becoming taut, five axons showed a measurable buildup of force that reached a steady value after ∼15–60 min. In the other axons, the force buildup could not be measured due to limitations in the sensitivity of the force sensors. Of interest, in three of the five axons where the force buildup could be measured, the steady-state value of the force was similar to the rest tension, whereas it was lower than the rest tension in the other two cases.

The increase in tension in two axons after unloading is shown in Fig. 3.6. The final tension in the first axon (Fig. 3.6*A*) was 1.77 nN (rest tension: 2 nN), whereas in the second axon (Fig. 3.6*B*) it was 2.77 nN (rest tension: 4.21 nN). At the end of the force buildup, the lengths of the first and second axons were respectively 10.2% and 47.6% larger than their initial lengths. Therefore, for both axons, although the final (equilibrium) length was larger, the force was smaller than the initial rest tension. This was the case for all five axons in which we could measure the force buildup. In contrast, for a standard viscoelastic solid in equilibrium, a larger length would always correspond to a higher force. Thus, unlike their elastic behavior and force relaxation response, the force generation of axons is not characteristic of standard viscoelastic solids. The fact that the final axonal tension never exceeds the rest tension suggests that the force buildup is a calibrated response of neurons to mechanical perturbation. In other words, neurons appear to actively regulate the tension in the axons in vivo.

3.4 Discussion

Our experiments show that *Drosophila* motor neurons maintain a rest tension in vivo and actively restore tension after being subjected to mechanical perturbation. The results clearly suggest that neurons regulate their tension in vivo. The force measurements further reveal that *Drosophila* neurons behave like viscoelastic solids under sustained stretching, i.e., they show a linear force-displacement response to fast stretching and exhibit force relaxation when the applied stretch is held constant.

These observations are in remarkable agreement with previous in vitro studies of cultured neurons. Dennerll et al. [1,9], for example, showed that both PC12 neurites and chick sensory neurons maintain a rest tension and have a linear relationship between force and length change when subjected to rapid distensions. These neurites also exhibited a viscoelastic response that is well described by the classical viscoelastic model of a stiff spring in series with a Voigt element comprised of a softer spring in parallel with a dashpot. In addition, PC-12 neurites that had become flaccid after stretch release shortened and became straight within a period of 5–15 min. This shortening was accompanied by an increase in tension to a value close to their rest tension [9]. Similarly, chick sensory neurons were also observed to actively generate tension in response to slackening, often to a value larger than their initial rest tension. Thus, the presence of a rest tension, viscoelastic behavior, and active force generation in response to loss of tension appear to be common elements of neuronal mechanical behavior both in vivo and in vitro.

Furthermore, tension appears to stimulate growth in *Drosophila* axons in a similar manner as it does in vitro. In a recent work, Lamoureux et al. [10] showed that in vitro axonal growth proceeds through a combination of steps, i.e., lengthening by viscoelastic stretching and intercalated addition of material. During viscoelastic stretching, a noticeable thinning of the axons was observed, but over a period of several hours the axons eventually regained their thickness by the addition of material. As shown in Fig. 3.5*C*, some *Drosophila* axons that exhibit large force relaxation also become noticeably thin during the process. The relaxation is accompanied by significant lengthening of the axon, which we interpret as the first stage of axonal growth. The decrease in their diameter also explains the reduction in their stiffness (Fig. 3.5*A*) during the next loading. On the other hand, *Drosophila* axons that show a relatively low force relaxation exhibit an increase in stiffness even though they also undergo a modest increase in length. Although this

may seem counterintuitive, the observations of Lamoureux et al. [10] provide a possible explanation for this increase in stiffness. They showed that addition of material to the axon, and consequently an increase in axon diameter, can precede the lengthening of axons in both spontaneously growing (growth cone-mediated) and towed axons. Such an addition of material, caused in our case by the externally applied force, would explain the increase in stiffness seen in some of the axons.

As noted above, the in vitro mechanical behavior of neurons has been studied extensively, and several models, both qualitative and quantitative, have been proposed to describe it. For example, Dennerll et al.[9] proposed a qualitative model in which the axonal response to tension is divided into three distinct phases. They suggested that when tension falls below a lower threshold, axons actively generate tension by contracting, whereas when tension exceeds a higher threshold, axons elongate to reduce tension. For intermediate values of applied tension, axons behave like passive viscoelastic solids. Recently, Bernal et al. [11] modeled axons as viscoelastic solids but added an extra element to mimic the action of molecular motors. They showed quantitatively that their extended model could predict several features of axonal contraction, at least for small deformations.

Although the macroscopic mechanical behavior of neurons is reasonably well understood, the cytoskeletal elements that underpin their behavior have yet to be unambiguously identified. In typical neurons, the axon cytoskeleton comprises a cortical actin network attached to the plasma membrane that runs parallel to a network of neurofilaments in which bundles of microtubules are embedded [12,13,14]. The viscoelastic behavior of axons is assumed to result from the elastic interactions and dissipation between these different cytoskeletal components. Among these components, the cortical actin network has been shown to be necessary for the elastic response of axons since their disruption by actin depolymerizing agents (such as cytochalasin D) significantly reduces the axon stiffness [9,15]. Through similar pharmacological interventions, microtubules have been shown to play a mainly structural role, undergoing assembly/depolymerization during growth/retraction without having any effect on the elastic behavior or viscoelastic response of axons [1]. However, the role of intermediate filaments (neurofilaments), which comprise a significant part of the axonal cytoskeleton, is still virtually unknown. Of interest, of the three major cytoskeletal elements, only intermediate filaments have been shown to sustain large deformation and forces [16,17 and 18].

In this context, our results showing that the behavior of *Drosophila* neurons is similar to that of other neurons become especially relevant. Because *Drosophila* is one of the most studied organisms, the organization and functioning of its nervous system is known in great detail. Furthermore, a myriad of sophisticated tools, including a wide array of genetic tools, are available to manipulate and probe them [19] Therefore, the molecular aspects of the mechanical behavior of *Drosophila* neurons can be examined in a degree of detail that is not possible with other types of neurons. Such detailed molecular investigations have the potential to unambiguously clarify the roles of different cytoskeletal elements in axonal response to tension. It is also worth noting that although there are many similarities in the behavior of *Drosophila* neurons and other types of neurites, there are significant differences in their cytoskeletal structures. For example, although the *Drosophila* axonal shaft is devoid of neurofilaments, it contains other filamentous networks [20]. The use of sophisticated molecular and genetic tools may be able to reveal what role, if any, these networks play in the mechanical response of neurons.

Although many questions remain about the cytoskeletal elements responsible for the viscoelastic behavior of *Drosophila* axons, their contraction behavior is consistent with the action of molecular motors. Experiments on cultured neurons have shown that axon contraction is mediated by tensile forces generated by the actomyosin contractile machinery. In the absence of tension, myosin motors can slide parallel F-actin filaments, and in the process shorten the axon [21]. During the free contraction of the *Drosophila*axons, there is no external force on the motors, and hence their velocity (and consequently the overall contraction rate) is constant (Fig. 3.7). However, the reason for the existence of two different contraction rates in some of the axons is unclear.

To summarize, in this work we examined behavior of axons in live *Drosophila* embryos using high-resolution micromechanical force sensors. Our experiments show that *Drosophila* neurons maintain a rest tension and actively regulate axonal tension in vivo. They also show passive viscoelastic behavior in response to applied deformation. These results are almost in exact agreement with the in vitro behavior of PC12 neurites and chick sensory neurons, and suggest that mechanical tension may strongly influence neuronal behavior in vivo. Given the vast knowledge of the organization and functioning of *Drosophila* neurons, and the genetic tools available to manipulate them, our results provide a platform to examine the molecular aspects of neuronal response to tension in detail.

3.5 Figures

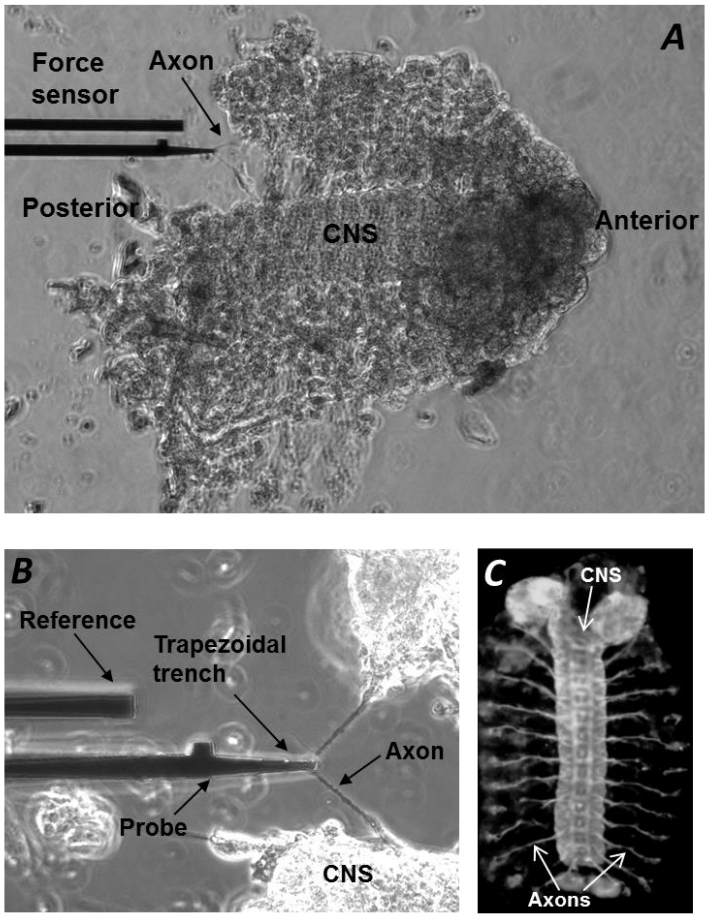

Figure 3.1: (*A*) Phase-contrast image showing a dissected embryo and the force sensor. As shown in the figure, axons close to the posterior of the embryo were usually isolated for the experiments. (*B*) A higher-magnification image of an axon being deformed by a force sensor. A trapezoidal trench was cut into the force sensor probe using focused ion beam milling to grip the axon. The principle of operation of the force sensor is explained in Fig.2.2. (*C*) Fluorescence image of the *Drosophila* embryo expressing GFP in all neuronal membranes.

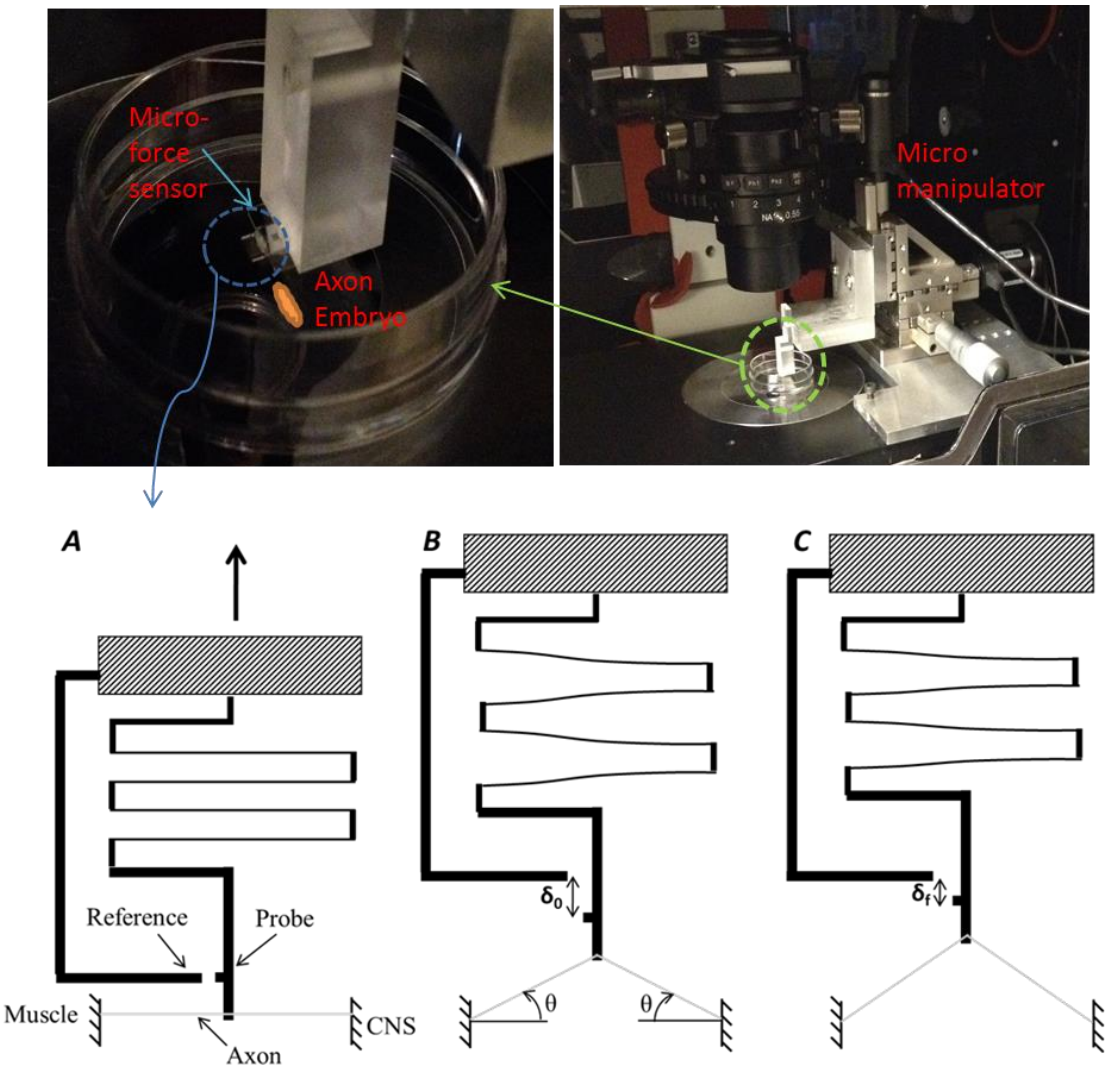

Figure 3.2: Schematic of the experiment used to measure the mechanical response of *Drosophila* axons. (*A*) Initial configuration of the force sensor and the axon. In this configuration, the force sensor is engaged to the axon but is not exerting any deformation. (*B*) In the first step, the axon is deformed by moving the force sensor away from the axon. The deflection of the probe (δ_0) with respect to the reference gives a direct measure of the force (F) acting on the probe. The tension (T) in the axon is then calculated from the force balance as T = F/2 sin θ. (*C*) When the force sensor is held fixed after loading, the tension in the axon relaxes. During this process the force on the probe reduces and the length of the axon increases. Note that the change in axon length is directly coupled to the deflection of the probe (δ_f).

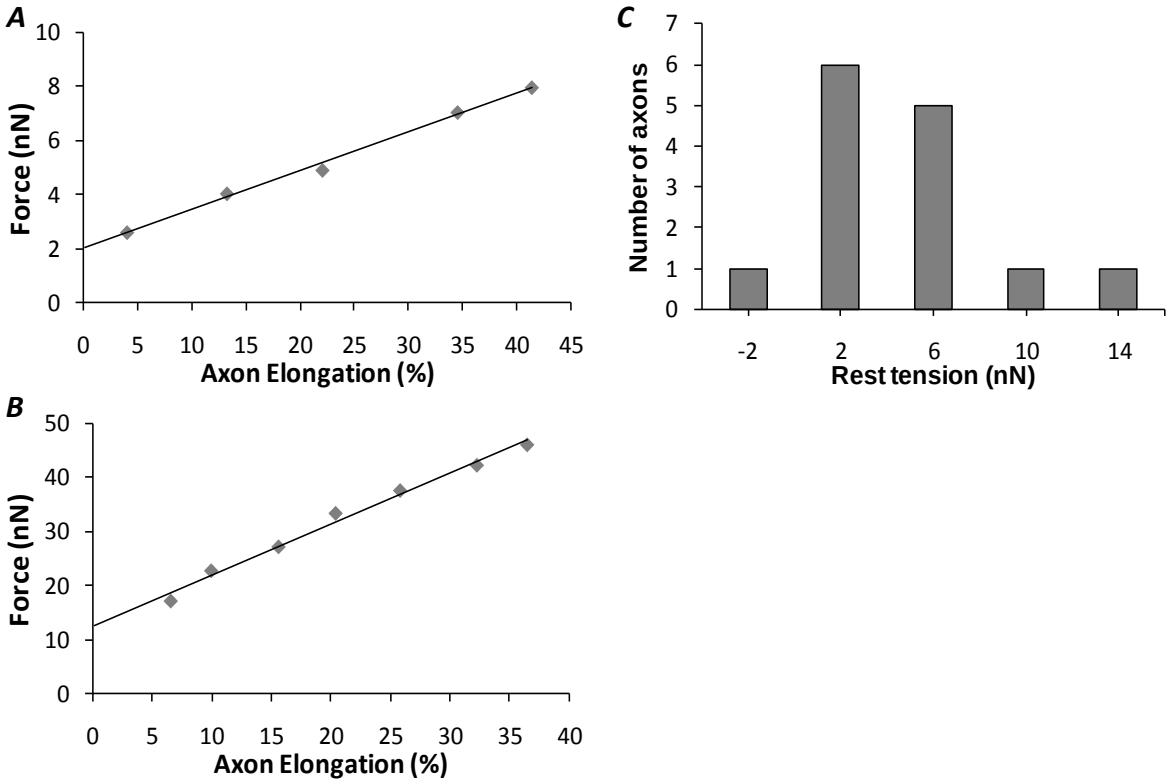

Figure 3.3: (*A* and *B*) The force-deformation response of two axons from different embryos during loading. Extrapolation of the force-deformation curve to zero deformation results in a positive force value in the axons, indicating the presence of a rest tension. (*C*) Histogram of axonal rest tensions.

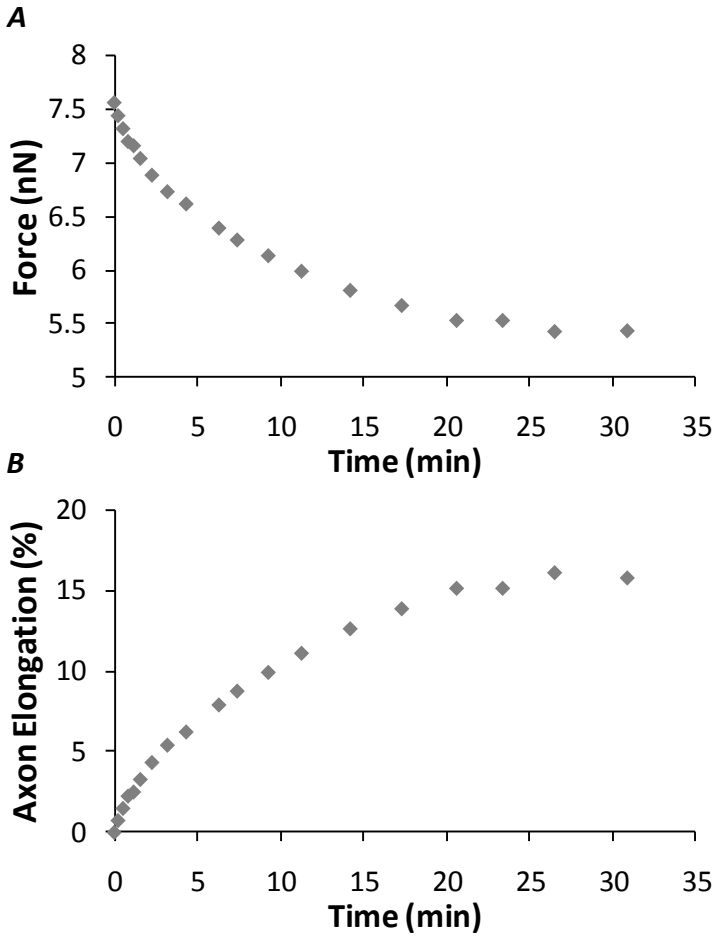

Figure 3.4: (*A*) Force relaxation in the axon whose loading response is shown in Fig. 3.3*A*. (*B*) Elongation of the axon during force relaxation. The plot of axon elongation over time mirrors the relaxation in force, since the axon length and the probe are coupled.

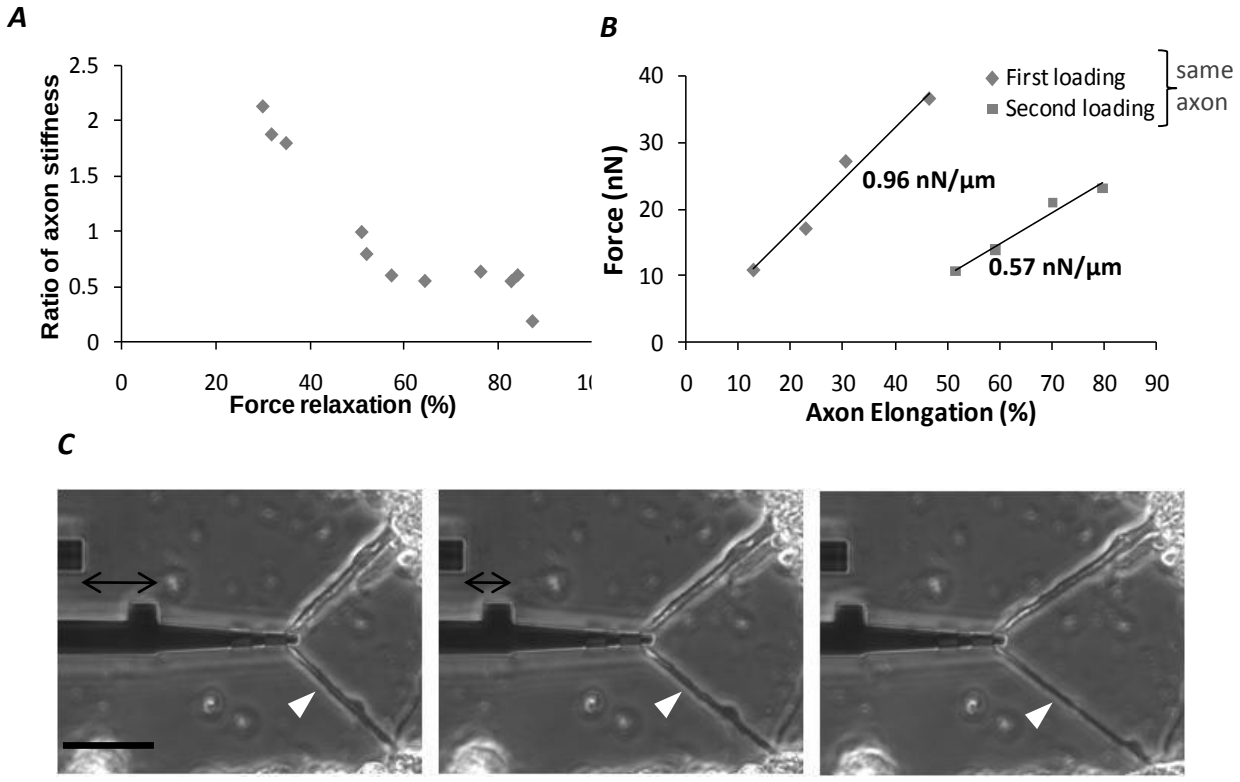

Figure 3.5: (*A*) Ratio of the stiffness of the axons during the first and second loadings plotted as a function of their force relaxation after the first loading. Axons that show a large force relaxation show diminished stiffness during the second loading, and vice versa. (*B*) Force-deformation response for the first and second loadings of an axon that underwent a large force relaxation after the first loading. (*C*) Thinning of the axon shown in *B* during force relaxation after the first loading. The reduction in diameter is especially pronounced in the lower half of the axon, as indicated by the arrowheads. The decrease in gap (indicated by double-headed arrows) between the reference and the probe shows the large decrease in force during relaxation. Scale bar = 35 μm.

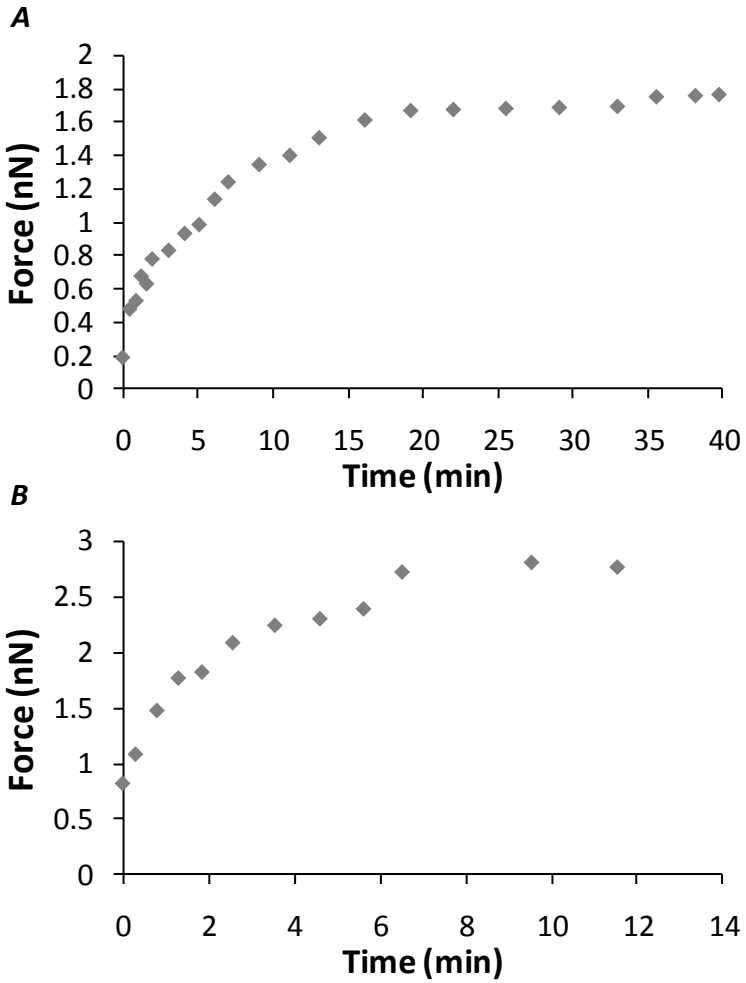

Figure 3.6: Force buildup in two axons after unloading. Part *A* corresponds to the axon whose loading curve is shown in Fig. 3.3*A*. Note that the tension in the axon after force buildup (1.77 nN) was close to its rest tension (2 nN). The tension in the axon shown in *B* after force buildup (2.77 nN) was lower than its rest tension (4.21 nN).

References

1. Dennerll, T. J., P. Lamoureux, R. E. Buxbaum, and S. R. Heidemann. 1989. The cytomechanics of axonal elongation and retraction. J. Cell Biol. 109:3073–3083.

2. Zheng, J., P. Lamoureux, ., S. R. Heidemann. 1991. Tensile regulation of axonal elongation and initiation. J. Neurosci. 11:1117–1125.

3. Heidemann, S. R., P. Lamoureux, and R. E. Buxbaum. 1995. Cytomechanics of axonal development. Cell Biochem. Biophys. 27:135–155.

4. Siechen, S., S. Yang, ., T. Saif. 2009. Mechanical tension contributes to clustering of neurotransmitter vesicles at presynaptic terminals. Proc. Natl. Acad. Sci. USA. 106:12611–12616.

5. Budnik, V., M. Gorczyca, and A. Prokop. 2006. Selected methods for the anatomical study of Drosophila embryonic and larval neuromuscular junctions. Int. Rev. Neurobiol. 75:323–365.

6. Ruiz-Canada, C., and V. Budnik. 2006. The Fly Neuromuscular Junction: Structure and Function. Academic Press, San Diego, CA.

7. Rajagopalan, Jagannathan, Alireza Tofangchi, and M. Taher A. Saif. "Drosophila neurons actively regulate axonal tension in vivo." *Biophysical journal* 99.10 (2010): 3208-3215.

8. Rajagopalan, J., A. Tofangchi, and M. T. A. Saif. 2010. Linear, highresolution BioMEMS force sensors with large measurement range.J. Microelectromech. Syst. 99. 10.1109/JMEMS.2010.2076780.

9. Dennerll, T. J., H. C. Joshi, ., S. R. Heidemann. 1988. Tension and compression in the cytoskeleton of PC-12 neurites. II: Quantitative measurements. J. Cell Biol. 107:665–674.

10. Lamoureux, P., S. R. Heidemann, ., K. E. Miller. 2010. Growth and elongation within and along the axon. Dev. Neurobiol. 70:135–149.

11. Bernal, R., P. A. Pullarkat, and F. Melo. 2007. Mechanical properties ofaxons. Phys. Rev. Lett. 99:018301.

12. Schnapp, B. J., and T. S. Reese. 1982. Cytoplasmic structure in rapidfrozen axons. J. Cell Biol. 94:667–669.

13. Hirokawa, N. 1982. Cross-linker system between neurofilaments,microtubules, and membranous organelles in frog axons revealed bythe quick-freeze, deep-etching method. J. Cell Biol. 94:129–142.

14. Alberts, B., A. Johnson, ., P. Walter. 2002. Molecular Biology of theCell. Garland Science, New York.

15. Joshi, H. C., D. Chu, ., S. R. Heidemann. 1985. Tension and compression in the cytoskeleton of PC-12 neurites. J. Cell Biol. 101:697–705.

16. Janmey, P. A., U. Euteneuer, ., M. Schliwa. 1991. Viscoelastic properties of vimentin compared with other filamentous biopolymernetworks. J. Cell Biol. 113:155–160.

17. Leterrier, J. F., J. Ka ¨s, ., P. A. Janmey. 1996. Mechanical effects ofneurofilament cross-bridges. Modulation by phosphorylation, lipids,and interactions with F-actin. J. Biol. Chem. 271:15687–15694.

18. Wagner, O. I., S. Rammensee, ., P. A. Janmey. 2007. Softness,strength and self-repair in intermediate filament networks. Exp. CellRes. 313:2228–2235.

19. Sanchez-Soriano, N., G. Tea, ., A. Prokop. 2007. Drosophila asa genetic and cellular model for studies on axonal growth. NeuralDevelop. 2. 10.1186/1749–8104–2–9.

20. Benshalom, G., and T. S. Reese. 1985. Ultrastructural observations onthe cytoarchitecture of axons processed by rapid-freezing and freezesubstitution. J. Neurocytol. 14:943–960.

21. Howard, J. 2001. Mechanics of Motor Proteins and the Cytoskeleton.Sinauer Associates, Sunderland, MA

Chapter 4

Dynamics of Axonal Contraction and Mechanism of Force Generation[1]

4.1 Motivation

We have previously observed that *Drosophila* axons actively maintain a rest tension of 1-13nN and axons that are made slackened become taut and restore a rest tension of similar magnitude in 10-30 minutes [1]. Contraction is also observed in neurites that are surgically severed. Earlier, Shaw et al. [2] described how isolated axon segments *in vitro* often shorten after they are resected. A number of *in vitro* studies have also demonstrated similar shortening behavior of axons upon surgical incision [3, 4, 5].

These results suggest that maintaining an intrinsic tension is an integral part of neural activities. In this study we address the question: what is the origin of tension in motor neuron axons? A surgically cleaned single-axon system in *Drosophila* enables us to simply bring the neuromuscular junctions closer to the central nervous system (CNS). Typically, in the absence of any drug, the axons shorten, become taut, and regain tension. This cycle of slackening and straightening can be repeated multiple times, resulting axons to shorten up to 40% of their original length in some embryos. The amount and rate of shortening are used as measures of contractility. We find that contractility decreases dramatically in the presence of myosin II inhibiting and actin disrupting drugs. The contractility however remains unaltered when microtubules are disrupted. These observations suggest that the acto-myosin machinery is primarily responsible in generating and regulating tension in *Drosophila* motor neurons.

1- Parts of this chapter are currently under review for publication as, Alireza Tofangchi, Anthony Fan, Taher Saif, "Mechanism of Axonal Contractility of Embryonic *Drosophila* Motor Neurons in vivo"

4.2 Materials and methods

Culture and Dissection of *Drosophila* embryos. Transgenic Drosophila (elav0-AL4/UAS-gap::GFP) expressing green fluorescent protein (GFP) in neuronal membranes were used for the experiments. The culture, preparation and dissection of embryos are exactly the same as outlined in [10]. In some cases, the axon of the RP2 neurons was also excised, leaving only the axon of the aCC neuron intact. In most cases, both axons were intact and we measured their combined response. Glass microneedles were fabricated using a Sutter Instruments (Novota, CA) laser-based micropipette/fiber puller.

Micromanipulator and Imaging. Actuation of the microneedle (Fig. 4.1B) was powered and controlled by an x-y-z piezo-actuator (NanoPZ PZC200; Newport, Irvine, CA). Live imaging of the axon under the applied deformation was carried out on an inverted microscope (IX81; Olympus, Nashua, NH). An Andor Neo sCMOS camera cooled to -30 ˚C was used to record images (Andor Technology, Belfast, UK) at 2 frames/second. Imaging parameters (e.g., light intensity, exposure time, gain, etc.) were kept constant during all experiments. Time-lapse images of axon contraction were analyzed by ImageJ (U.S. National Institutes of Health, Bethesda, MD).

Axon compression and contraction measurement. In order to relax the axonal shaft, a microneedle tip was gently placed on the tissue embedding the NMJs as shown in Fig. 4.1A. The tissue was then pushed towards the central nervous system (CNS) by 10-15% of initial axon length, L_0. This caused the axon to become slack. Note that L_0 is the arc length between two identifiable markers (a and b, in Fig. 4.1A) on the axon immediately after a push, and not necessarily the length between the CNS and the NMJ. We denote the straight-line distance between the two markers by L_s. Immediately after slackening, the axon started to shorten its length to a final length L_f within 2-4 minutes (Fig. 4.1C). We call this entire process of slackening and shortening a compression cycle. If the axon resumes the taut configuration by the end of the compression cycle then $L_f = L_s$, otherwise, $L_f > L_s$. Multiple compression cycles can be applied to the axon, as will be discussed later. The symbols used for measuring axon contraction are listed in Table 4.1.

Table 4.1: List of symbols used in the axon compression experiment

Parameter	*Definition*
L_0	Measured arc length of axon from point a to b (Fig 4.1 A) immediately after push
L_f	Measured arc length of axon from point a to b 5 minutes after push
L_s	Straight-line distance between points a and b: ideal length of taut axon
C_r	Contraction factor $\frac{\Delta L_f}{\Delta L_0} = \frac{L_0 - L_f}{L_0 - L_s}$ represents normalized magnitude of axonal contraction
τ	Time constant of axonal contraction by assuming a first order decay
ΔT	Time interval between each compression cycle

Drug Treatments. Embryos were treated with specific pharmaceutical drugs at certain concentrations under controlled scheme described in the following sections. These includes 2Deoxyglucose and Sodium Azide for ATP depletion (n=6) [10], Blebbistatin for inhibition of Myosin II activity (n=5) [11], ML-7 to inhibit Myosin light chain kinase MLCK (n=2) [12], Y-27632 to inhibit Myoisn Rho kinase ROCK (n=2) [12], Latrunculin A, an agent to disrupt cortical actin (n=3) [13,16] and Cytochalasin D for disruption of F-actin (n=3) [14], Nocodazole and Colchicine to disrupt microtubule filament (n=2) [15], all prepared from Sigma Aldrich. DMSO is added as a solvent and is maintained at a final concentration of less than 5%. All drugs are diluted in Ca^{2+}/Mg^{2+}–free PBS.

4.3 Results

4.3.1 Contraction behavior of intact axons

Axons have robust contraction ability upon sustained loss of tension. In this section, we investigated:

1) Whether embryonic *Drosophila* axons are capable of generating contractile force after they undergo mechanically induced loss of tension
2) The dynamics of such contraction due to multiple successive compression cycles.

Figures 4.2A & B respectively show the experimental steps and the fluorescent images of a representative axon subjected to three compression cycles. To remove tensile force in axonal shaft, the axon was compressed from the NMJ side, which caused the axon to buckle and become slack (push 1). But the axon exhibited gradual self-shortening (contraction) and ultimately reached a stable straight (length L_f) configuration within 2-3 min (end of compression cycle 1). The degree of contraction for each axon in the cycle is characterized by the contraction factor C_r defined as,

$$C_r = \frac{\Delta L_f}{\Delta L_0} = \frac{L_0 - L_f}{L_0 - L_s} \tag{4.1}$$

Here $0 \leq Cr \leq 1$, and $C_r = 0$ indicates no contraction ($L_0 = L_f$), $C_r = 1$ indicates full contraction ($L_f = L_s$, see Fig. 4.1 and Table 4.1). Three embryos were investigated and all showed high degree of contraction, with C_r = 90–95% in cycle 1. In order to investigate whether the shortened axons can further contract when subjected to another compression cycle, we examined the same axon for a

2nd compression cycle (push 2) after one hour ($\Delta T_1 = 1hr$). The axon reached a steady state and became fairly straight within 2–4 minutes with C_r = 80–90%. Finally, the same axon was pushed for the 3rd cycle (push 3) after half an hour ($\Delta T_2 = 0.5hr$, Fig. 4.2A & B). Again, shortening occurred within 2–4 minutes with a C_r close to those in previous cycles. This is consistent among all three embryos examined (Fig. 4.2C). Note that because the axon length decreased at the end of each compression cycle, the value of L_0, L_f and L_s vary among compression cycles. It is also worth noting that the total compressive strain (based on L_0 in cycle 1 and L_f in cycle 3) exceeds 40% in some embryos, although axon length varied from 70 μm to 105 μm from embryo to embryo. These results show the rapidness and robustness of axon shortening and tension regulation in response to multiple occasions of loss of tension. Results here will also serve as our control data for the later sections where embryos are subjected to various pharmaceutical treatments.

Axon contraction shows exponential decay over time with less shortening rate in 2nd compression cycles. To study the dynamics of Drosophila axon contraction, we monitored time lapsed images of axons and measured their instantaneous change of length over time during both the 1st and 2nd compression cycles. The time-dependent contraction can be fitted to a first order exponential equation as:

$$L(t) = L_f + \left(L_0 - L_f\right) e^{-t/\tau} \tag{4.2}$$

$$\Delta L(t) = L(t) - L_0 = -\Delta L_f \left(1 - e^{-t/\tau}\right) \tag{4.3}$$

where $L(t)$ is the instantaneous length, $\Delta L_f = L_0 - L_f$ is total contraction of the axon, τ is the time constant. We obtain the time constant τ by fitting the experimental data to the exponential curve (Fig. 4.3A). τ and C_r (Eq. 1) represent the two independent parameters characterizing the rate and magnitude of axon contraction in a given compression cycle. We find that all axons exhibit a generic exponential decay in shortening over time in both cycles (Fig. 4.3B). However, contractions in the second cycle have a slower rate consistently among embryos (Fig. 4.3C, n=3). Note that C_r is similar in both cycles and seems to be independent of τ.

4.3.2 Contraction behavior of axons subject to drugs treatments

In order to explore the mechanism of axonal contraction, we investigate contraction response of axons subjected to various pharmaceutical drugs. Each drug has potent ability to impair/disrupt specific cellular activity/structure in axons as discussed in the following sections. Results for contraction of intact axons in compression cycle 1 and 2 (Fig. 4.2) in the absence of any drugs are used as control data. Specifically, drug experiments were carried out in three steps (Fig. 4.4):

1. The intact axon was compressed and its subsequent contraction was monitored. This is identical to compression cycle 1 in control. Total time of this phase that axon became taut was within 4 minutes
2. The embryo was treated with specific drug at a prescribed concentration. An hour ($\Delta T = 1hr$) was allowed for the drug to act on the axon.
3. The same axon was examined for the 2nd compression cycle and its subsequent contraction response was monitored for 5 minutes (end of experiment).

Note that the time interval $\Delta T = 1hr$ is similar to that in control, and the axon was monitored for 5 minutes after push 2 which is more than the time required for the intact axon to reach a steady state in the absence of drug.

Axons contraction is active and requires metabolic energy to create tension. In order to investigate whether the process of axon contraction is active and hence requires metabolic energy, the embryos were treated as outlined in 3.2 (n=6) with combined 2Deoxyglucose (60 mM, 1 hr) and Sodium Azide (20 mM) in order to deplete ATP [10]. As expected in the first cycle, the axon contracted with $C_r = 0.81 \pm 0.12$ within 2 minutes, while in the second cycle, the contraction factor noticeably dropped to $C_r = 0.13 \pm 0.08$ (Fig. 4.5A). Thus ATP inhibitory reagent significantly impairs axon contraction suggesting that axonal contractility is an active process supported by metabolic energy. We further hypothesize that ATP specifically drives myosin II to mediate axon contraction, and hence the impairment of myosin II motors will lead to similar result as in ATP depletion. We aim to verify this in the next section.

Myosin II contributes to force generation in axons through MLCK and ROCK pathways. We investigated the role of Myosin II in axon contraction using different inhibitory reagents, each following the same procedure in 3.2. In the first set of experiments, the embryos were treated with Blebbistatin (n=5, 83 μM, 1 hr), a potent inhibitor of Myosin II [11]. We observed significant inhibition of axon contraction (C_r = 0.10 ± 0.06) in the 2nd cycle compared to the first cycle (no drug, C_r = 0.87 ± 0.07), indicating that Myosin II mediates axons contraction (Fig. 4.5B).

To further identify the molecular pathways by which Myosin II is activated in axons, we separately treated the embryos (as outlined in 3.2) with reagents ML7, an inhibitor of Myosin light chain kinase MLCK [3] (n=2,225 μM, 1 hr), and Y-27632, an inhibitor of Rho-dependent kinase [12] (n=2, 110 μM, 1 hr). Both ML7 and Y-27632 reduced axon contraction in the 2nd cycle, with C_r = 0.21 ± 0.01 and 0.15 ± 0.04 respectively (Fig. 4.5C &D). When both drugs were used simultaneously, the inhibitory effect was much more pronounced (not shown). These results together indicate that both MLCK and ROCK pathways contribute to Myosin-based contraction and force-generating machinery in live *Drosophila* axons (Fig. 4.5E).

Axon contraction stopped upon disruption of F-action/cortical actin but remained insensitive to disruption of microtubule filaments. Myosin motors employ actin filaments to generate intracellular tension. Therefore, if myosin II is indeed involved is axonal contractility, then disruption of actin filaments should also result in loss of contractility. To examine this hypothesis, embryos were separately treated with Cytochalasin D (50 μg/mL, n=2) and Latrunculin A (31 μM, n=2), the potent reagents that disrupt F-actin[22] and cortical actin [21, 24]respectively. As it is evident in Fig. 4.6A, both Cytochalasin D and Latrunculin A significantly impair the ability of axons to contract, characterized by the reduced values of C_r = 0.09±0.04 and C_r = 0.12±0.04 in the 2nd cycle respectively. When both drugs were used simultaneously, the inhibitory effects were more pronounced (not shown).

Since the axonal shaft is abundant with microtubule filament (MT), we ask whether MT has any direct role in axonal contraction. To address this question, the embryos were simultaneously treated (n=2) with Nocodazole (15 μg/mL) and Colchicine (200 μM), potent drugs to destabilize microtubule filaments [14, 25]. After drug treatments, axons maintain a high Cr = 0.80 ± 0.02 in

the 2nd cycle, similar to the control data, indicating that axon contraction is insensitive to MT disruption (Fig. 4.6B) as typically observed in *in vitro* experiments [17].

4.4 Discussion

Our experiments reveal that *Drosophila* motor neurons *in vivo* are capable to contract and straighten their length within 2-4 min after they are mechanically slackened. This contractility appears to be robust, i.e., axons contract in the 2nd and even the 3rd compression cycle with a C_r close to 1, regardless of their initial length and time interval between cycles as shown in Fig 4.2 B & C. The axons do not show any memory of their past contraction cycles. The total contraction often exceeded 40% of the initial length in our experiments. This process cannot be characterized by a passive response of viscoelastic materials, which we further confirm by depleting ATP. Without ATP, axonal contraction fully stopped (C_r value close to 0), and axons never returned to straight configuration. This confirms that neurons utilize metabolic energy to contract and generate tensile force in axonal shafts. The ATP dependence of contraction has also been reported in DRG chicken neuron *in vitro* [4]. Thus, active contractility appears to be an evolutionarily conserved property of neurons both in vivo and in vitro.

Our observations on axonal contractility in embryonic Drosophila are in good agreement with previous *in vivo* findings [1] where neurons were subjected to only one compression cycle, and the axon restored tension by shortening. The value of the tension (measured by a micro probe in [1]) after compression was similar to the rest tension that the axon maintained prior to the compression cycle. In fact, axons not only can contract and restore tension after first compression [1], but they can further contract upon three consecutive compression cycles (current work). This suggests that axonal contraction can be regarded as a force regulatory mechanism and stops when tension reaches a threshold value.

The time evolution of axon contraction in each cycle is analogous to that of a system modeled by a first order decay equation (Fig. 4.3A & B), suggesting that contractile machinery in axon consists of internal elasticity and dissipative elements, both working against internal generative forces (motor protein) and external stimulation (slackening caused by displacement of NMJ towards

CNS). In addition, the reduction in axon contraction rate (or increase in time constant) in the successive compression cycles indicates a possible increase in frictional forces in axonal shaft. This reduction in contraction rate is likely due to the formation of a denser filamentous network upon axon shortening, since the cytoskeletal elements is known to be one of the major sources of internal friction in axon [15]. Interestingly, although the contraction rate decreases in successive compression cycles, axons ultimately restore their straight configuration and possibly the rest tension [1]. In effect, this behavior suggests the presence of an active stretch-control mechanism in axons that, in spite of increased internal resistance, consistently operates sometime at the cost of delayed recovery.

Several investigations have been performed to unravel the underlying mechanism of motility in neurons in vitro, i.e., growth, elongation and retraction. These studies have shed light on the role of cytoskeletal structure and motor protein activity in contractility of axon in different types of neurons. For Instance, in vitro studies demonstrated that disruption of F-actin eliminates retraction of neuritis [3,19]. Similarly, It is also shown that depolymerization of actin networks lead to a significant reduction in the rest tension in axons [26]. Our findings agree with these results in which actin is observed to actively participate in contraction dynamics-contraction factor *Cr* abruptly dropped to 12% after actin filament were disrupted (Fig 4.6)

Motor protein also have significant role in force generation and motility of axon. For example, it has been observed that retractions in chick sensory neurons [19], Neuro–2A neurites [12], and DRG neurons [3] are significantly dependent on Myosin II. These agree with our observations that Myosin II plays a major role in contraction dynamics: Axon contraction was significantly impaired when Myosin II was inhibited using pharmaceutical reagents that targeted motors and MLCK cascade (Fig. 4.5B). This, combined with our results on actin disruption (Fig. 4.6), strongly suggests that the interplay of acto-myosin machinery drives the dynamics in active contraction of slackned axons. It is also conceivable that actin network serves as force conduit along the axonal shaft. They can sustain and transmit both external force [6] and internally-generated tension (by Myosin motors, current work); and hence, once disrupted, contractility significantly dropped in axons.

It has been shown that microtubules passively counterbalance tensile forces along the F-actin. For instance, disruption of microtubules in axons led to an increase in rest tension [5, 18]. In other studies, destabilization or stabilization of microtubules resulted in enhanced or retarded recovery rate of dynamically-stretched axons respectively [15]. These evidence show that microtubules mechanically oppose the neuron-generated tension forces. Our results show no significant changes in the magnitude of axon contraction when microtubules were disrupted in embryonic flies. We however did not measure the rest tension subsequent to contraction and cannot draw direct comparison with the in vitro studies..

Maintaining tension might be vital for the functionalities of ion channels. It has been argued that all ion channels are mechanosensitive—a large enough stress will induce conformational change in ion channels which would lead to an increase/decrease in their activation energy barrier for conductance [20]. Thus, it is conceivable that tension generated by acto-myosin machinery might serve as a signal for the ion channels, which in turn may influence polymerization of cytoskeletal components and motor activity. Thus, the channels and actomyosin machinery may act as feedback loop system maintaining the rest tension and resulting an optimal condition for neuronal function.

It has been suggested that cortical folding in cerebral cortex of large mammals could be driven by intrinsic axonal tension aiming to pack the most neurons in a confined space, i.e. efficient wiring [21]. Several efforts have been attempted to prove this hypothesis [22, 23]. Most experimental results suggest that intrinsic tension does not cause cortical folding, but no evidence has so far concluded against its role in efficient wiring.

As is evident from some previous experiments [24, 25], neurons respond to mechanical stimuli quite significantly. However, neuron, like any long wire, can only sense mechanical signal when it is tensed. The ultimate role of tension homeostasis of neurons may not merely be limited to growth as is conventionally understood, but might be related to various neuronal functions, including axonal transport, synaptic transmission and excitability. Taken together, tension might be related to memory and learning.

4.5 Figures

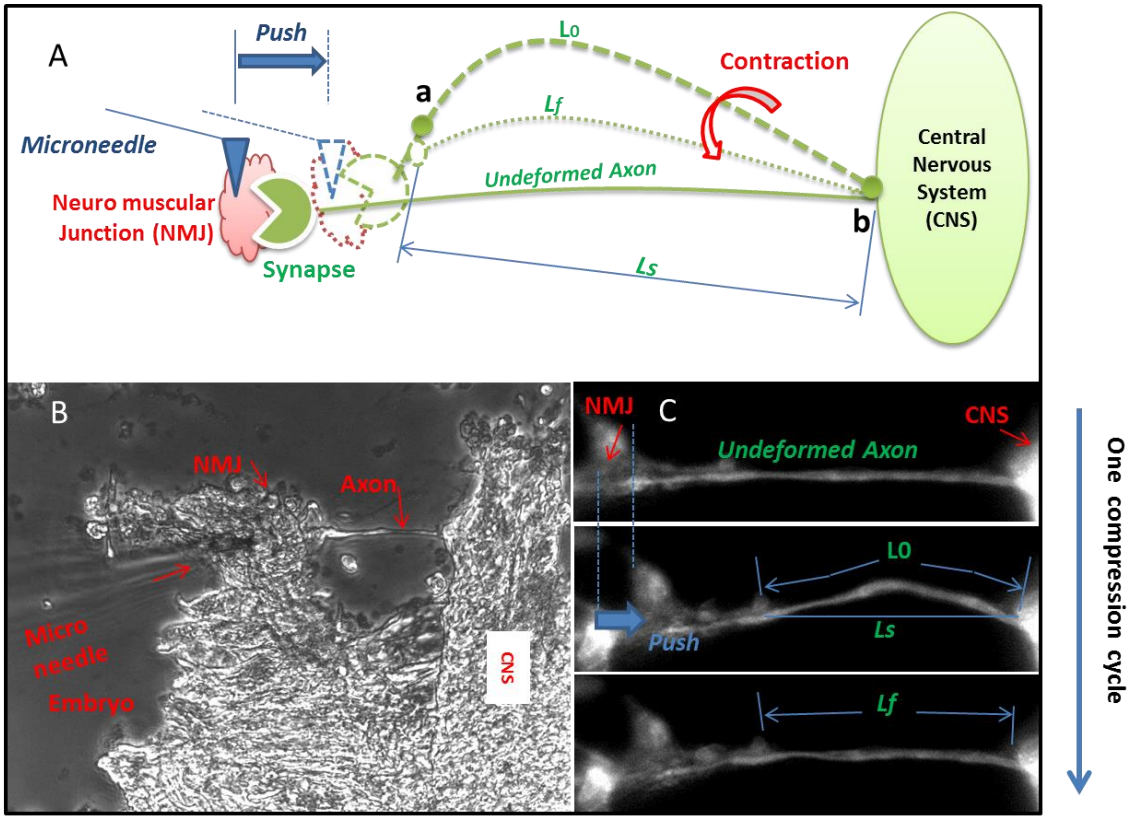

Figure 4.1: (A) Schematic of experiments on single axons of embryonic *Drosophila*. Geometrical parameters used to analyze contraction behavior in each axon are labeled. (B) Phase contrast image of dissected embryo. The axon is being pushed with the microneedle from its NMJ end. (C) The geometrical parameters are labeled on the fluorescent image of an axon undergoing a complete slackening cycle.

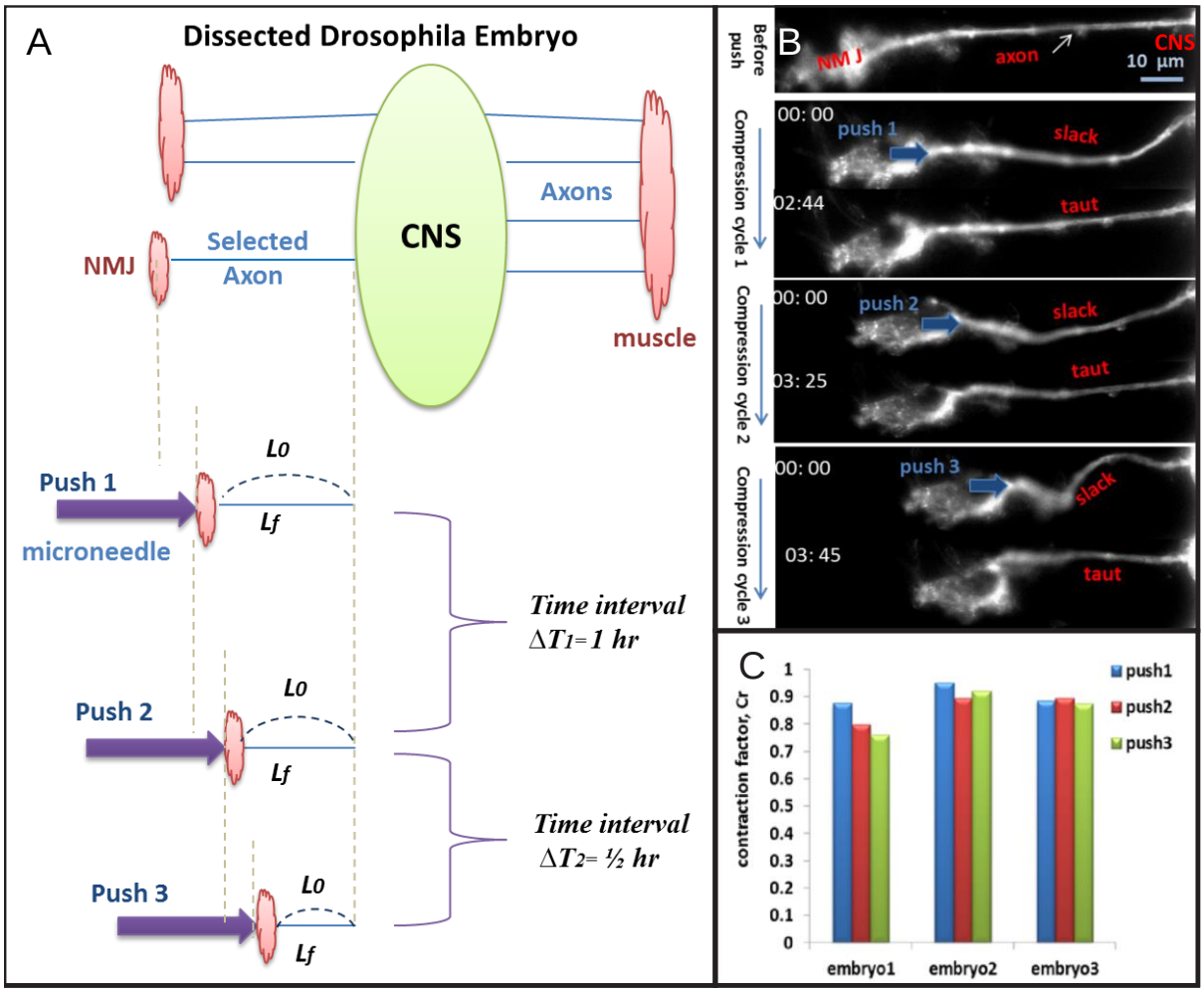

Figure 4.2: (A) Schematic showing the sequence of three slackening cycles. In each cycle, axon with an initial length *L*0 slackens and gradually contracts to a taut configuration of final length *Lf*. Note that *L*0 and *Lf* are different in each cycle, while the range of *Cr* remains the same ($0 \leq Cr \leq 1$). $\Delta T1$ = 1 hour, $\Delta T2$ = 0.5 hours are time intervals between the cycles. (B) Experimental images showing an axon contract during three consecutive slackening cycles. The contraction strain in each cycle is 10–15% of initial length (*L*0 in each cycle). Note that axon contracts and becomes taut upon each push within 2–4 minutes. Total shortening is about 40% of original length (*L*0 in cycle 1). (C) Three embryos are examined under the same condition (3 consecutive pushes) and contraction factors in all three cycles are calculated. All axons contract successively within 4 minutes.

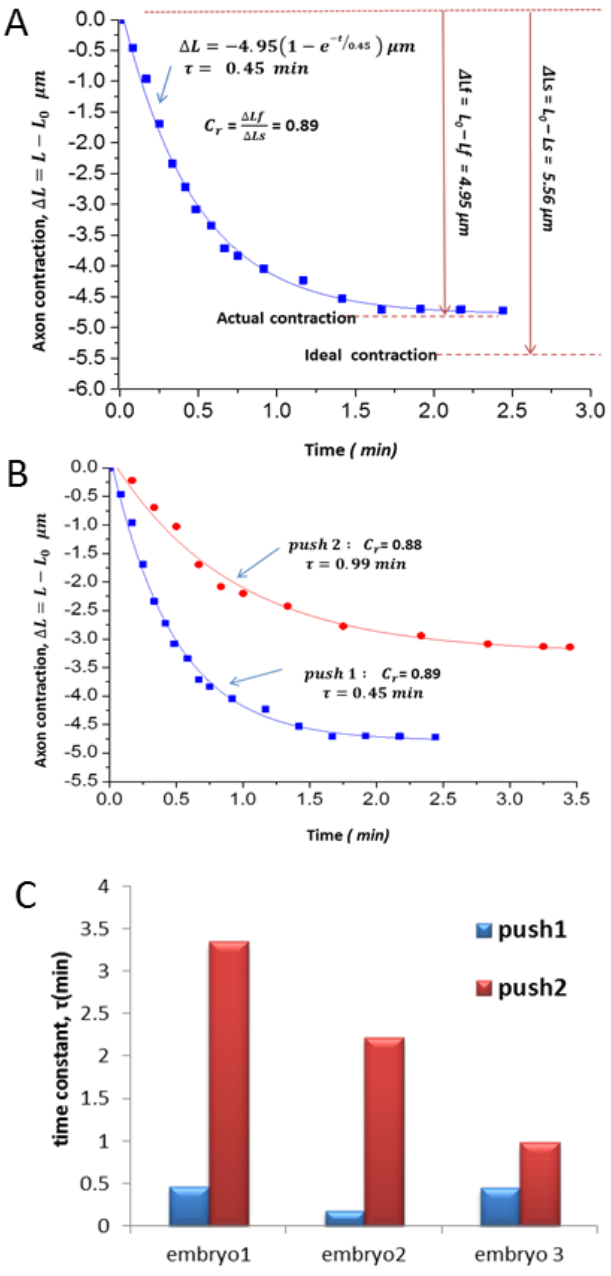

Figure 4.3: (A) Time-dependent length reduction of an intact axon (embryo 3) upon slackening can be characterized by an exponential function and time constant τ can be extracted thereafter. (B) & (C) Axons contract at a slower rate (higher time constant) in the 2nd compression cycle compared to that in the 1st cycle, while contraction factor *Cr* remains similar

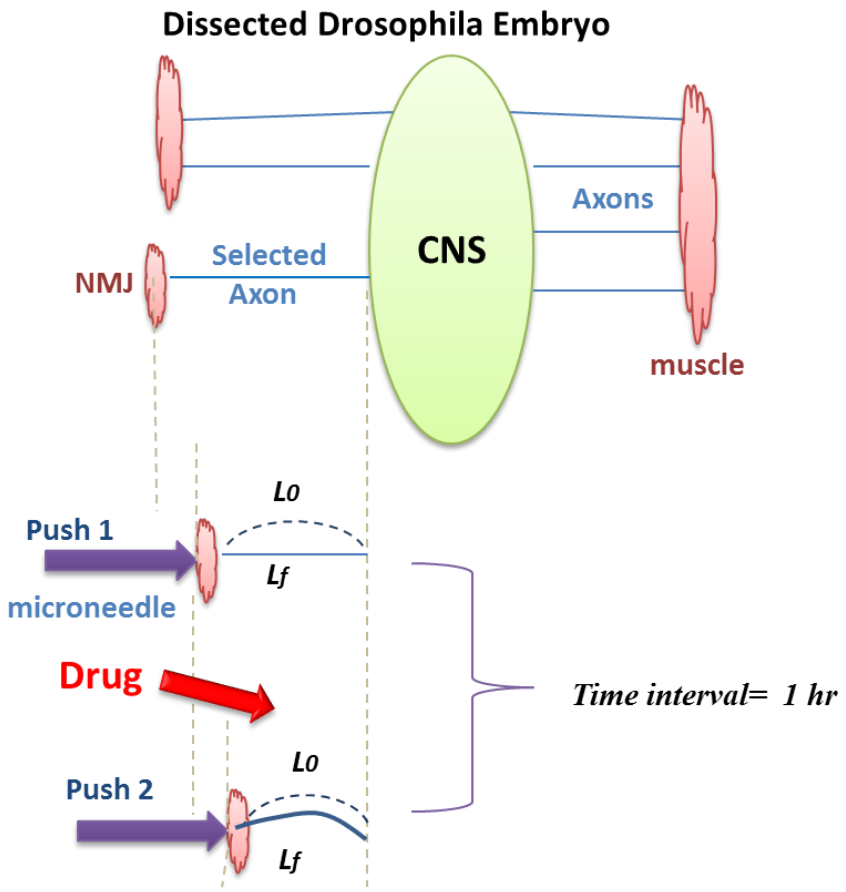

Figure 4.4: Schematic showing the procedure for pharmaceutical manipulations. Push 1 is performed exactly as before. Selected drugs are added after push 1 and incubated for $\Delta T = 1hr$, after which axon underwent push 2. Note that the time interval (ΔT) between pushes is 1 hour, similar to that in control. 3rd push was not applied in experiments with drugs.

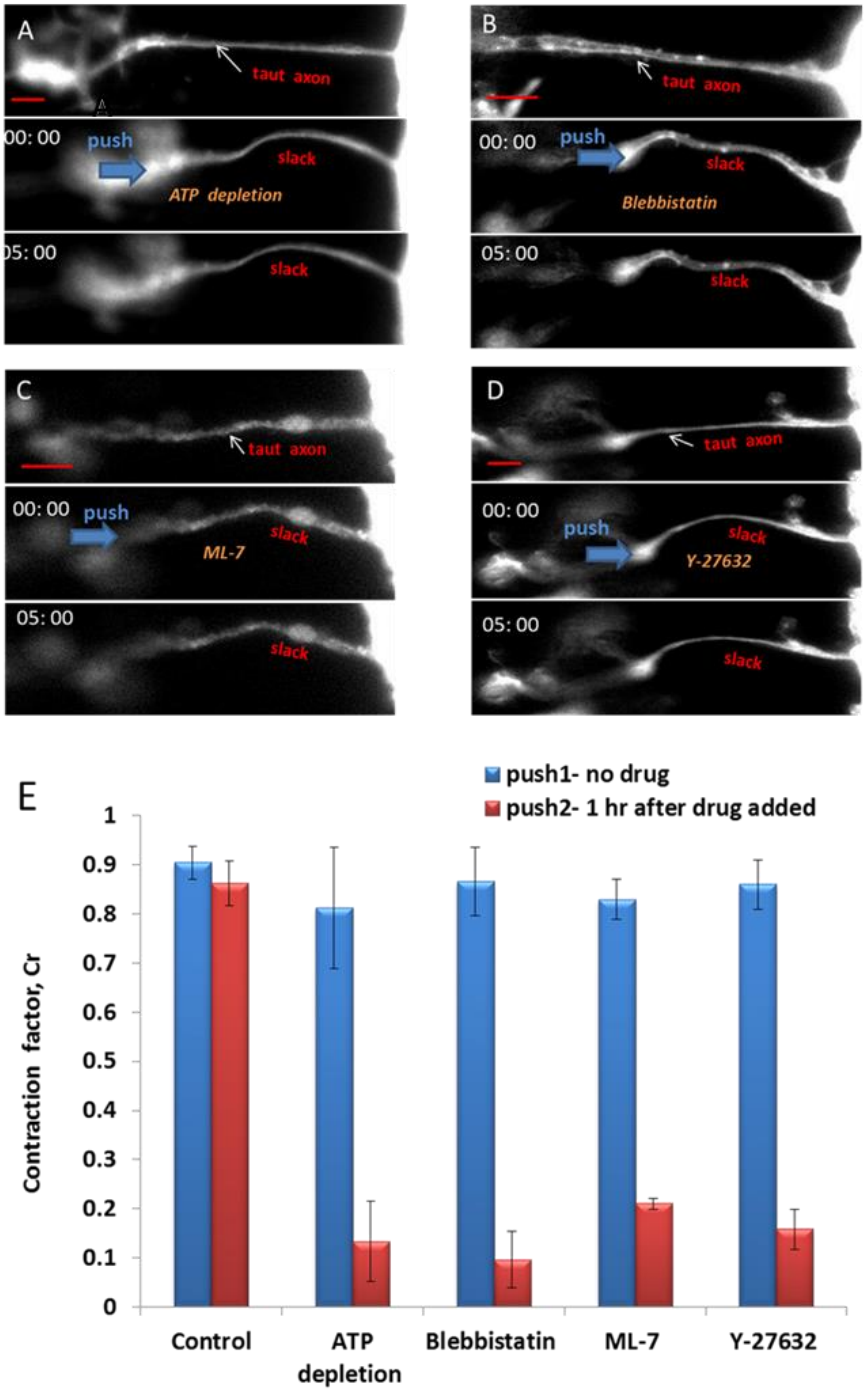

Figure 4.5: (A) Axon contraction stops when ATP is depleted by treating embryos with 2Deoxyglucose and Sodium Azide. This indicates that axon contraction is active and needs metabolic energy (n=6). Similarly, axons stops to contract when Myosin II is inhibited by (B) Blebbistatin (n=5), (C) ML7 (MLCK pathway, n=2), and (D) Y-27632 (ROCK pathway, n=2). (E) Summary of results suggesting that myosin is involved in active force generation in *Drosophila* axons. Note that no drugs are used in control cases. Scale bar = 10 μm

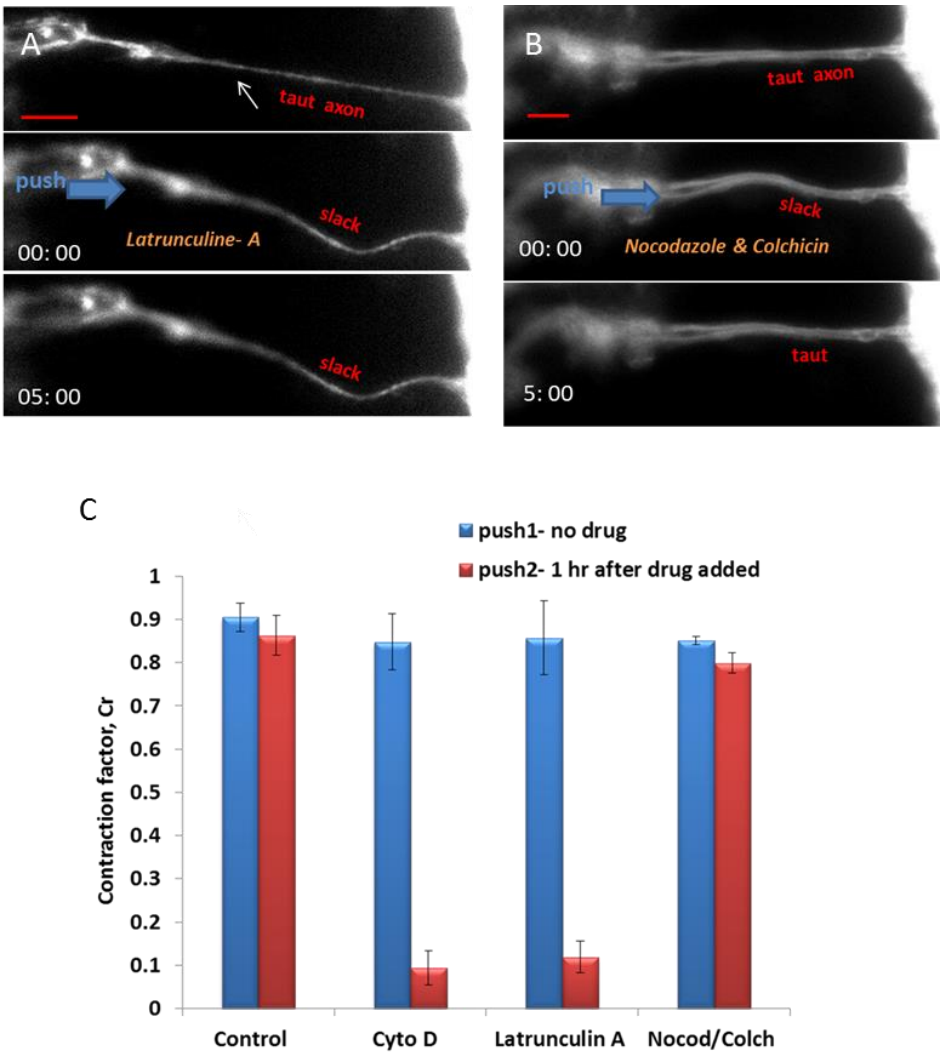

Figure 4.6: (A) Axon contraction is significantly inhibited when embryo is treated with Cyto D (n=3) and Latrunculine A (n=3). (B) Axon contraction remains unaffected, as compared to control cases, when embryos are treated with Nocodazole and Colchicin combined (n=2). (C) Summary of results shows a significant decrease in axon contraction when actin structures are disrupted while axon contraction remains active and is insensitive to disruption of microtubule filaments. No drugs are used in control cases. Fig. 4.5 and 4.6 together implicate actomyosin machinery as the primary mechanism of axonal contractility in embryonic *Drosophila*. Scale bar = 10 μm.

References

1. Jagannathan Rajagopalan, Alireza Tofangchi, and M Taher A Saif. Drosophila neurons actively regulate axonal tension in vivo. Biophysical journal, 99(10):3208–15, November 2010.

2. G Shaw and D Bray. Movement and extension of isolated growth cones. Experimental cell research,104(1):55–62, January 1977.

3. Gianluca Gallo. Myosin II activity is required for severing-induced axon retraction in vitro. Experimental neurology, 189(1):112–21, September 2004.

4. E B George, B F Schneider, R J Lasek, and M J Katz. Axonal shortening and the mechanisms of axonal motility. Cell motility and the cytoskeleton, 9(1):48–59, January 1988.

5. H C Joshi, D Chu, R E Buxbaum, and S R Heidemann. Tension and compression in the cytoskeleton of PC 12 neurites. The Journal of cell biology, 101(3):697–705, September 1985.

6. T J Dennerll, P Lamoureux, R E Buxbaum, and S R Heidemann. The cytomechanics of axonal elongation and retraction. The Journal of cell biology, 109(6 Pt 1):3073–83, December 1989

7. W W Ahmed, T C Li, S S Rubakhin, A Chiba, J V Sweedler, and T A Saif. Mechanical tension modulates local and global vesicle dynamics in neurons. Cellular and molecular bioengineering, 5(2):155–164, June 2012.

8. Anthony Fan, Kevin Stebbings, Daniel Llano, and Taher Saif. Stretch induced hyperexcitability of mice callosal pathway. bioRxiv, 2015.

9. Vivian Budnik, Michael Gorczyca, and Andreas Prokop. Selected methods for the anatomical study of Drosophila embryonic and larval neuromuscular junctions. International review of neurobiology, 75:323–65, January 2006.

10. M P Sheetz, N L Baumrind, D B Wayne, and A L Pearlman. Concentration of membrane antigens by forward transport and trapping in neuronal growth cones. Cell, 61(2):231–41, April 1990.

11. Mih´aly Kov´acs, Judit T´oth, Csaba Het´enyi, Andr´as M´aln´asi-Csizmadia, and James R Sellers. Mechanism of blebbistatin inhibition of myosin II. The Journal of biological chemistry, 279(34):35557–63, August 2004.

12. Steven R Wylie and Peter D Chantler. Myosin IIA drives neurite retraction. Molecular biology of the cell, 14(11):4654–66, November 2003.

13. I Spector, N R Shochet, D Blasberger, and Y Kashman. Latrunculins–novel marine macrolides that disrupt microfilament organization and affect cell growth: I. Comparison with cytochalasin D. Cell motility and the cytoskeleton, 13(3):127–44, January 1989.

14. J A Cooper. Effects of cytochalasin and phalloidin on actin. The Journal of cell biology, 105(4):1473–8,October 1987.

15. Min D Tang-Schomer, Ankur R Patel, Peter W Baas, and Douglas H Smith. Mechanical breaking of microtubules in axons during dynamic stretch injury underlies delayed elasticity, microtubule disassembly,

and axon degeneration. FASEB journal : official publication of the Federation of American Societies for Experimental Biology, 24(5):1401–10, May 2010.

16. J A Lunn, H Wong, E Rozengurt, and J H Walsh. Requirement of cortical actin organization for bombesin, endothelin, and EGF receptor internalization. American journal of physiology. Cell physiology, 279(6):C2019–27, December 2000.

17. F J Ahmad, C J Echeverri, R B Vallee, and P W Baas. Cytoplasmic dynein and dynactin are required for the transport of microtubules into the axon. The Journal of cell biology, 140(2):391–401, January 1998.

18. T J Dennerll, H C Joshi, V L Steel, R E Buxbaum, and S R Heidemann. Tension and compression in the cytoskeleton of PC-12 neurites. II: Quantitative measurements. The Journal of cell biology,

107(2):665–74, August 1988.

19. F J Ahmad, J Hughey, T Wittmann, A Hyman, M Greaser, and P W Baas. Motor proteins regulate

force interactions between microtubules and microfilaments in the axon. Nature cell biology, 2(5):276–80, May 2000.

20. Frederick Sachs. Stretch-activated ion channels: what are they? Physiology (Bethesda, Md.), 25(1):50–6,February 2010.

21. D C van Essen. A tension-based theory of morphogenesis and compact wiring in the central nervous system. Nature, 385(6614):313–8, January 1997.

22. Gang Xu, Philip V Bayly, and Larry A Taber. Residual stress in the adult mouse brain. Biomechanics and modeling in mechanobiology, 8(4):253–62, August 2009.

23. Gang Xu, Andrew K Knutsen, Krikor Dikranian, Christopher D Kroenke, Philip V Bayly, and Larry A Taber. Axons pull on the brain, but tension does not drive cortical folding. Journal of biomechanical engineering, 132(7):071013, July 2010.

24. Scott Siechen, Shengyuan Yang, Akira Chiba, and Taher Saif. Mechanical tension contributes to clustering of neurotransmitter vesicles at presynaptic terminals. Proceedings of the National Academy of Sciences of the United States of America, 106(31):12611–6, August 2009

25. B M Chen and A D Grinnell. Integrins and modulation of transmitter release from motor nerve terminals by stretch. Science (New York

Chapter 5

Diametric Regulation of Single Axons Induced by Mechanical Stretch[1]

5.1 Motivation

We previously showed that single axons of embryonic *Drosophila* straighten and restore tension in response to slackening; relax and approach a new rest tension in response to stretch (chapter 1 4 and [1]) This was shown also by the active contraction of the acto-myosin machinery

Because of existing strong evidences showing that axons are able to regulate forces along their axonal shaft both in vivo and in vitro [2,3,4], it is plausible that to hypothesize when the axons are subjected to tension or force relaxation, their cytoskeletal structure undergo reorganization [5] or mass addition/transport occurs along the axon. This internal volumetric process can be externally manifested as an increase or decrease in diameter for mechanically perturbed axons. In this study, we investigate the cytoskeleton and motor protein interaction through monitoring the diameter of a single axon in embryonic *Drosophila in vivo*.

5.2 Materials and methods

Drosophila culture, dissection and micro-manipulation. Transgenic Drosophila (elav0-GAL4/UAS-gap::GFP) expressing green fluorescent protein (GFP) in neuronal membranes were used for the experiments. The culture, preparation and dissection of embryos are exactly the same as outlined [1].

1-Parts of this chapter are currently under review for publication as , Anthony Fan, Alireza Tofangchi, M. T. A. Saif, "In vivo Regulation of Axonal Diameter Induced by Mechanical Stretch in *Drosophila* Embryos.

Pharmaceutical drug. Blebbistatin (83 μM) was used for the inhibition of Myosin II activity. Cytochalasin D (50 μg/mL) was used for the disruption of F-actin. Nocodazole (15 μg/mL) and Colchicine (200 μM) were used for the disruption of microtubules. All chemicals were purchased from Sigma-Aldrich (St. Louis, MO). Drugs were left incubated for 1 hour in all experiments before any further manipulations. DMSO was added as a solvent and was maintained at a final concentration of less than 5%. All drugs were diluted in Ca^{+2}/Mg^{+2} free PBS.

Confocal imaging. The above setup was set under a confocal microscope (LSM700; Zeiss, Oberkochen, Germany) (Fig. 5.1B). The 488-nm laser was used to excite the GFP and emission light with wavelength larger than 488 nm was collected. Pinhole size was set to 1 a.u.. A z-stack distance of 0.41 μm was maintained. We note that the number of images (ranges from 15-50) within every stack was different mostly because of the out-ofplane tilting of the axon (Fig. 5.1C). We discarded samples with too much tilting. The resolution and scan averaging were adjusted so that an image stack could be obtained in around 80 seconds. The setting was kept consistent in each independent experiment. We found that this minimized photobleaching while allowing good-quality images. Image stacks were taken either every 2 minutes, 5 minutes, or 15 minutes to maximize data collection and minimize photobleaching.

Image analysis. The collected images were post-processed first using ImageJ (U.S. National Institutes of Health, Bethesda, MD). The z-stacks were collapsed to single images by maximum intensity projection. The images were cropped to only the axon of interest which were then transferred to MATLAB (MathWorks, Natick, MA). A batch-enabled script was used to detect the edge of the axons, and subsequently performed diameter and area calculations (Fig. 5.1D). The edge was traced by fitting a Gaussian profile to the intensity profile along the x-axis for every y-intercept. The 2 locations with maximum slope ($\frac{d^2I}{dx^2}$= 0) were reported for each y-coordinate. Connecting those points for all y-coordinates provided a discretized edge with axial (y-) resolution of a single pixel. 3D images were generated by Image J.

5.3 Results

The experiments were performed by first stretching the axon to 20-25% strain. The axon was then held stretch for 30 minutes before unloaded back to the original position. It would become slack initially yet straightened again in the course of 2-3 minutes (ref). We traced the dynamics for another 30 minutes after straightening (Fig. 5.2A-1). In some cases the stretch was maintained for 60 minutes and no unloading was performed. For experiments with drugs, an incubation period of 45-60 minutes would precede the stretching manipulation (Fig. 5.2A-2). Two sets of control experiments were performed: 1) dissected and mounted embryos with no stretching/drugs manipulations (Fig. 5.2A-3); 2) dissected and mounted embryos (no drugs) with stretching manipulations delayed for 45 minutes (Fig. 5.2A-4). Confocal image stacks were collected throughout in all experiments.

Volume conservation in diameter regulations. If we consider, during initial loading, the CNS→MN→NMJ system to be purely passive and movement of mass is slow such that it is a closed system, then conservation of volume should apply given a Poisson's ratio of 0.5 (incompressible). This is only true during the initial loading period, because a living system is not passive. This is also only true when the fast dynamics will not lead to a significant instantaneous influx/outflux of mass. We verify such conservation of volume during initial loading by comparing the theoretical change in average diameter to experimental values. Given the definition of strain (ε) as $\frac{\Delta l}{l}$, stretch ratio (λ) is defined as:

$$\lambda_m = \frac{l_m}{l_0} = \frac{l_0+\Delta l}{l_0} = 1 + \epsilon_m \qquad m = 1,2, \text{etc} \tag{5.1}$$

where m is the stage number assuming a multi-stage stretching process. The volume ratio for a cylindrical rod is then:

$$\frac{V_m}{V_0} = \frac{{d_m}^2}{{d_0}^2}\left(\frac{l_m}{l_0}\right) = \frac{{d_m}^2}{{d_0}^2}\ \lambda_m \tag{5.2}$$

If volume is conserved, then volume ratio is 1. The inverse diameter ratio is then:

$$\frac{d_0}{d_m} = \sqrt{\lambda_m} = \sqrt{1+\varepsilon_m} \tag{5.3}$$

Two strain measurements were used to calculate the respective diameter ratios. One, termed globalstrain, traces the 2 ends of the axon; the other, termed local strain, traces 2 clearly identifiable points along the axon (Fig. 5.2B). The result for one axon is shown in Fig. 5.2C. As the data suggest, it is in close agreement with volume conservation. We can only show 1 axon due to different applied strain among experiments and the difficulty to normalize such, but all experiments show similar trend during initial loading.

Dynamics when subjected to stretch cycle. After verifying volume conservations during initial loading, we look into the response of lateral regulation, i.e. average diameter change. This relies on the fact that the CNS and NMJ are well adhered to the glass slide for fixed end points. Data from Fig.5.2A-1 &5.3 are presented where incubation medium is just PBS. Average diameter of each axon is then traced over a period of 60 minutes unless disrupted during the process. Results are normalized to respective starting average diameter immediately after the stretching manipulations. All traces are plotted in Fig. 5.3A, where the stretch group showed a significant reduction in diameter as compared to the control group. In a portion of the stretched experiments, the axon was brought back to its original end points (restoration), i.e. CNS and NMJ returns to the same position as before the stretch manipulations. The axon was consequently slackened, but would straighten within 2-3 minutes. Diameters just before slackening and right after straightening observe volume conservation. However, at a longer time-scale, restoration (unloading) surprisingly *enhances* reduction in diameter as compared to those axons that remain stretched (Fig. 5.3B). We further plotted the diameter (not averaged) along the entire axonal length for 3 time points in all experiments (one example shown in Fig. 5.3C). It is observed that this regulation in diameter in the stretched group happens along the entire length—neither within a specific region, nor polarized towards the CNS/NMJ side (Fig. 5.3D).

Under the influence of pharmaceutical drugs. We postulate that this regulation is predominately dictated by the activities of cytoskeleton structures and their response to external load. To identify specific responsible member so that we can develop a conceptual model, we employed 3 sets of pharmaceutical drugs to target specific elements in the cytoskeleton architecture. The addition of blebbistatin, inhibitor of myosin II, and Cytochalasin D, inhibitor of actin polymerization, completely reverses the phenomenon observed in the previous section. During the initial incubation period, as depicted in Fig. 5.2A-2, the average diameter

increases steadily (Fig. 5.4A). Once stretch is applied and held, the diameter keeps on increasing at a slower rate (Fig. 5.4B). The addition of a mixture of colchicine and nocodazole, both distablizing agent of microtubules assembly, during incubation reduces the diameter as opposed to the control and the blebbistatin group (Fig. 5.4A). Once stretch is applied and held, the diameter keeps on decreasing at a faster rate (Fig. 5.4B), but slower when compared to the stretch group with no drugs (Fig. 5.3B). No significant difference can be observed in the restoration phase between the 3 drugs (Fig. 5.4C). As in the previous section, we plot the diameter (not averaged) along the entire axonal length for 3 time points. A set of data from the blebbistatin group is presented here (Fig. 5.4D). This upward regulation in diameter, similar to the reduction (Fig. 5.3D), happens along the entire length—neither within a specific region, nor polarized towards the CNS/NMJ side (Fig. 5.4E).

5.4 Discussion

The diametric dynamics that occur during the course of our experiments reveal something about the responsible cytoskeletal members. Upon treating with blebbistatin and cytochalasin D, the diameter increased during the incubation phase. This suggests that intact acto-myosin machinery is constantly applying a circumferential pressure. Note that if the acto-myosin network has no preferred direction of alignment, it would also imply that a tension along the axial direction is maintained. In fact, this rest-tension phenomenon is well established *in vitro* and *in vivo* across species, and has also been shown dependent on activities of actin filaments and myosin motors. Incubation with microtubules destabilizing drugs led to an active decrease in diameter. This suggests that as microtubules destabilize, there is less resistance against acto-myosin constriction hence diameter is reduced. It seems that both diameter and the level of rest tension could be regulated this way by allowing equilibrium at different concentrations of force generators (actin filaments & myosin motors) and supportive structures (microtubules).

Previous observations on contraction of a slackened axon suggest that there exist internal dissipative elements inside an axon. Dissipations could come from the internal friction of the sliding microtubules and also from cross-linkers among microtubules. In the case with microtubules disrupting drugs in our current work, the diameter of the axons reduced to beyond that required by volume conservation. The magnitude of decrease is however less than that of

untreated cases. It seems to us that when the microtubules are stabilized, they cannot achieve a packed state as easily as in untreated cases. The exact mechanism is not conclusive, but one possible explanation is that the cross-linkers coupling the untreated microtubules are rotated during a sustained stretch leading to a smaller gap between them. This mechanism is perturbed in treated case leading to a comparatively larger gap among microtubules and therefore smaller decrease in diameter. Acto-myosin disruption on the other hand, leads to a slight increase on average which suggests that the circumferential relaxation continues but is slowing down.

None of the treated cases show any diametric regulation upon restoration, while in the untreated cases diameter further reduced post-restoration. The disruptions on acto-myosin machinery limits the axon to impose any circumferential pressure like in all other cases. Disruption of microtubules, however, did not significantly impair the regulation in previous cases, which suggests that the slackening process has caused it to interfere with acto-myosin contraction. This is based on evidences from other studies which showed that microtubules do not participate actively in contractions. Combined with the post-restoration diametric decrease in untreated case, we arrive to the conclusion that during the slackening process, microtubules are fragmented and rotated. Without inhibition drug, they would reorganize and subsequently allowing actomyosin to contract and hence result in a reduction in diameter. Microtubules inhibition drugs prevent this reorganization process from happening.

The reduction in diameter might seem counterintuitive to normal development since one would expect the axon to grow. In fact, several *in vitro* experiments have shown that axons when towed would grow both axially and laterally. However, the stretch is imposed slowly and gradually throughout the course of the experiment in those studies, while in our case the time from no stretch to full stretch (20% of original length) is usually within 10 seconds. This seems to suggest that different scales of mechanical input has vastly different results. Axons might first constrict when a sudden stretch occurs (naturally or artificially) to relieve pressure from surrounding tissue. Then as stronger mass reaccumulates, which possibly has a longer time scale than what our system can capture, it starts to regrow. The study of development is a multi-scale problem in which it could be a rather slow and lasting process at times, yet fairly rapid and sudden at other times. It is thus important to understand the full spectrum of mechanical effects before a solid conclusion could be drawn.

5.5 Figures

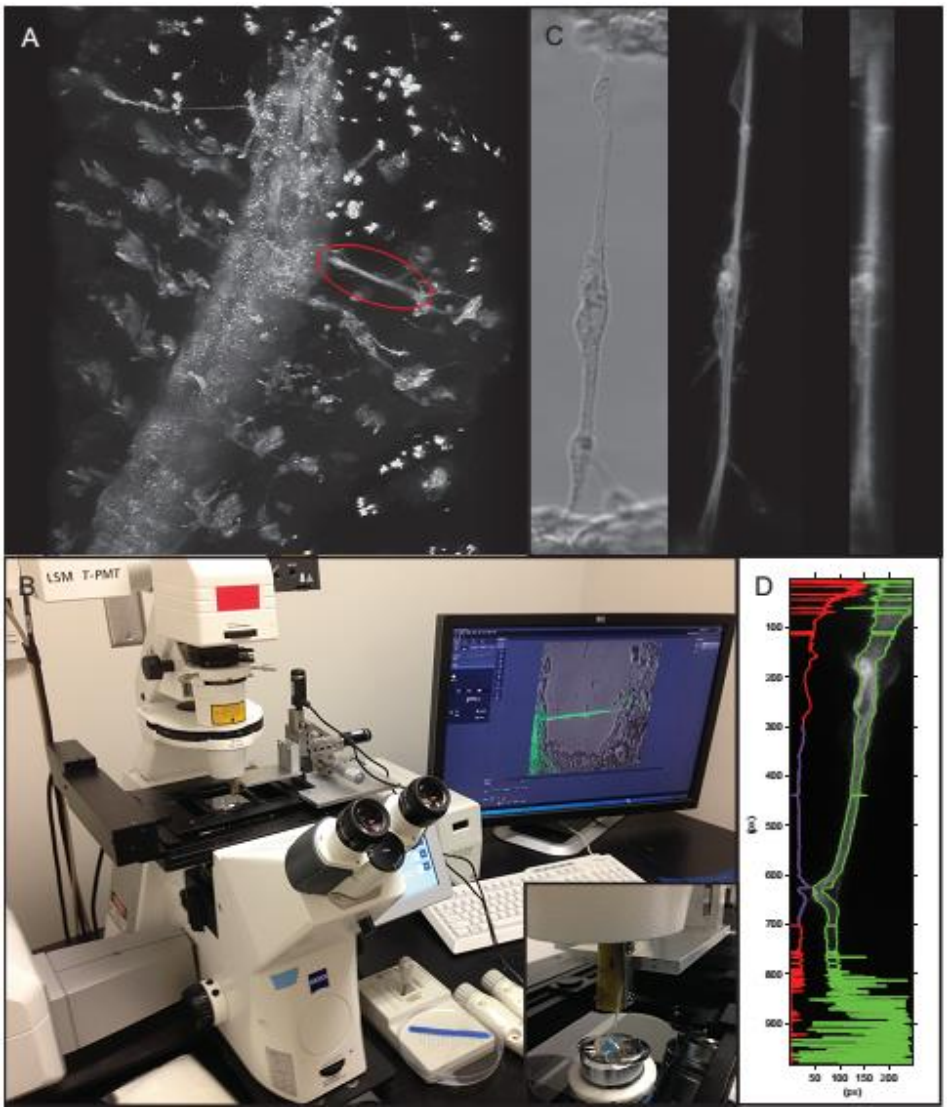

Figure 5.1: Manipulations, imaging, and analytical methods. (A) A tilted 3D reconstruction of a confocal stack of the red circle indicates a cleaned axon after dissection. As apparent, it is impossible to do any quantify cation without the surgical manipulations. (B) Setup of the experiment. (C) (left) DIC image of a cleaned axon. (center) Maximum-intensity-projected GFP image of the same axon. (right) The same axon looking from the side view (y-z plane, made available by the confocal stack). Notice how it is tilted, indicating that the axon is not parallel to the x-y plane. (D) Quantications using algorithms written n MATLAB. Green lines highlight the computed edge. Red line indicates the distance between te green lines, hence diameter. Purple line indicates the corrected diameter accounting for the in-plane rotation. As fluorescence signal fades, the computation is noisy (y=800-1000 px). The algorithm is also robust with axon before self-straightening has occurred such as the one shown (x=100 px, y=600 px). We, however, only use straightened axon because tension state in slack ones is undetermined.

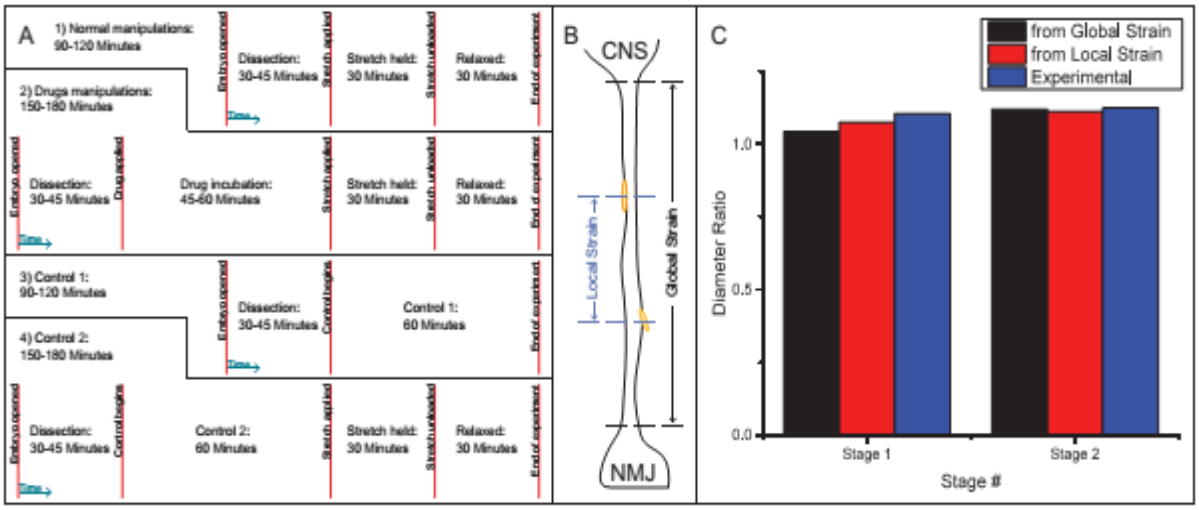

Figure 5.2: (A) Schematics and flow of all experiments. All experiments are completed within 3 h rs from dissection to end of data collection to minimize impact of health deterioration of the animal. (B) Schematics of the 2 methods in quantifying strain. (C) Two stages of stretching are performed. Both stages showed experimental consistency with the theoretical diameter ratio indicating volume is largely conserved during initial loading.

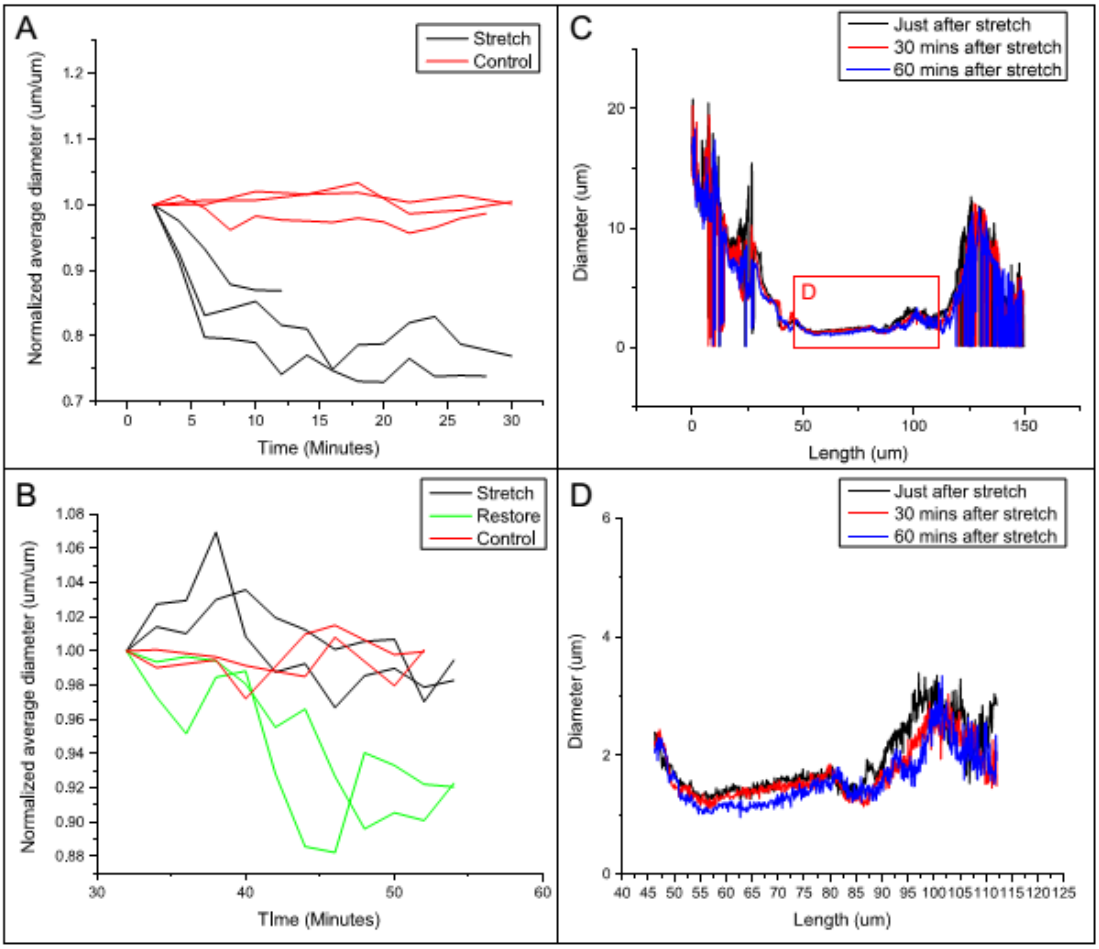

Figure 5.3: Diameter regulation in normal PBS. (A) Average diameter vs time plot in stretched and control groups when stretch is held. (B) Average diameter vs time plot in stretched and restored groups when stretch is either held or completely released. (C) Diameter along the axonal length for one set of data in the stretched group. The noisy ends are due to weaker fluorescence signal (blocked by surrounding tissue) and non-Gaussian cross-sections. (D) Expanded view of a section labeled in C where data describe the axon.

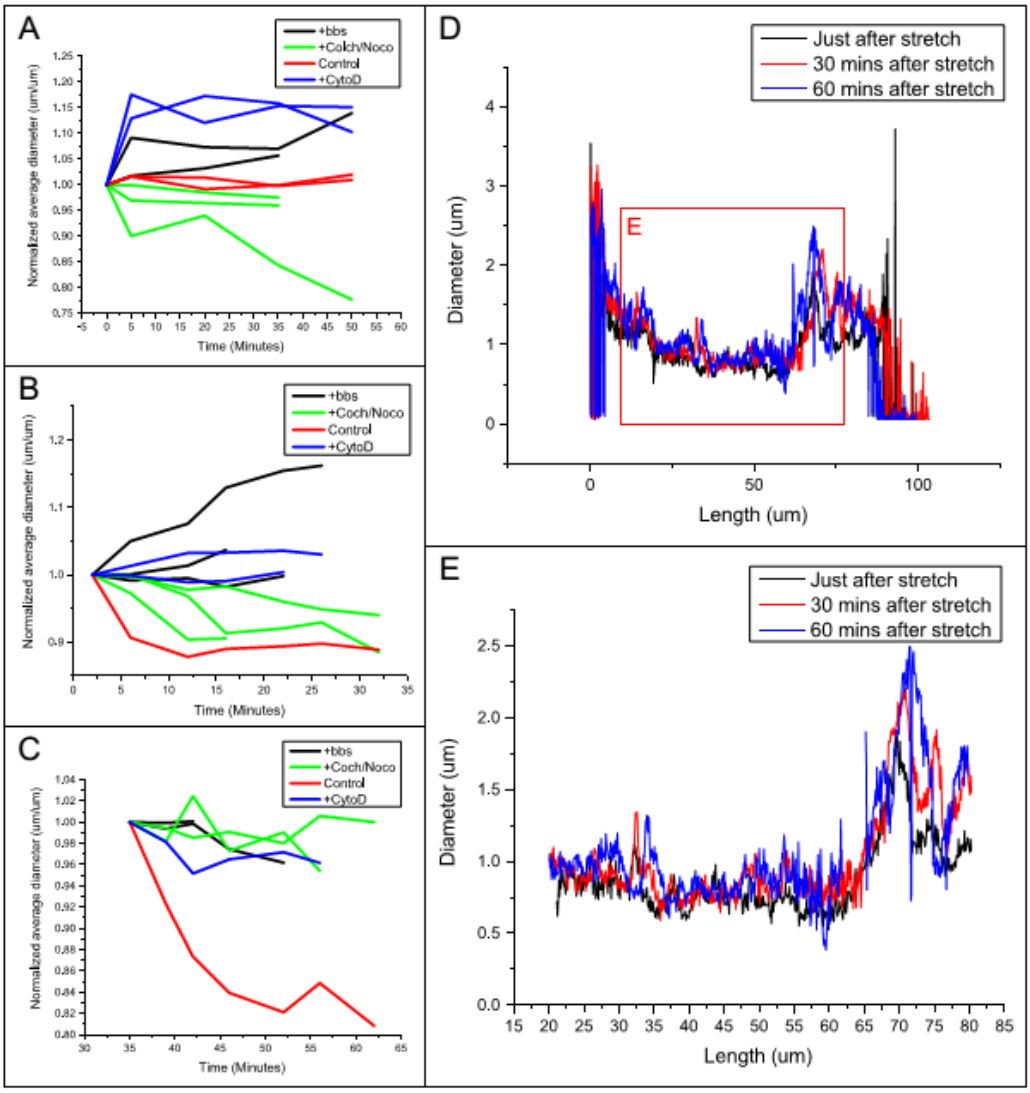

Figure 5.4: Diameter regulation in PBS with various drug. (A) Average diameter vs time plot in groups with blebbistatin (+bbs) and a mixture of colchicine and nocodazole (+Coch/Noco) added. No stretching manipulations are performed. (B) Average diameter vs time plot for groups in A when stretched. (C) Average diameter vs time plot when drugged axons are restored to initial length. (D) Diameter along the axonal length for one set of data in the blebbistatin group. The noisy ends are due to weaker fluorescence signal (blocked by surrounding tissue) and non-Gaussian cross-sections. (E) Expanded view of a section labeled in D where data describe the axon.

References

1. Jagannathan Rajagopalan, Alireza Tofangchi, and M Taher A Saif. Drosophila neurons actively regulate axonal tension in vivo. Biophysical journal, 99(10):3208–15, November 2010.

2. T J Dennerll, H C Joshi, V L Steel, R E Buxbaum, and S R Heidemann. Tension and compression in the cytoskeleton of PC-12 neurites. II: Quantitative measurements. The Journal of cell biology,

3. H C Joshi, D Chu, R E Buxbaum, and S R Heidemann. Tension and compression in the cytoskeleton of PC 12 neurites. The Journal of cell biology, 101(3):697–705, September 1985.

4. T J Dennerll, P Lamoureux, R E Buxbaum, and S R Heidemann. The cytomechanics of axonal elongation and retraction. The Journal of cell biology, 109(6 Pt 1):3073–83, December 1989

5. F J Ahmad, C J Echeverri, R B Vallee, and P W Baas. Cytoplasmic dynein and dynactin are required for the transport of microtubules into the axon. The Journal of cell biology, 140(2):391–401, January 1998

Chapter 6

Concluding Remarks and Outlook

This dissertation presents an experimental investigation to explore how embryonic *Drosophila* motor neurons regulate axonal tension *in vivo*. This work also attempts to address the origin of neuron-generated forces at the molecular and cytoskeletal level. In part, this research further involves with the techniques for development and fabrication of a micro force sensor and micro manipulation devices in order to perform experiments.

First, a set of displacement-based high resolution (50 pN) micromechanical force sensors (MEMS) with a large force measurement range (1 μN) was designed and fabricated (Chapter 2) . The sensors are composed of a series of flexible beams attached to a rigid probe that deform when subjected to an external force. The force sensors are fabricated using a simple two-mask process that allows for their stiffness to be varied over a wide range while remaining in linear range.

The device was then used to study the mechanical response of motor neurons in live *Drosophila* embryos (chapter 3). The results revealed that *Drosophila* neurons maintained a rest tension (1–13 nN) and behaved like viscoelastic solids (i.e., with a linear force-deformation response followed by force relaxation to steady state) in response to sustained stretching. More importantly, when the tension was suddenly diminished by a release of the externally applied force, the neurons contracted and actively generated force to restore tension, sometimes to a value close to their rest tension. These observations are remarkably similar to results from in vitro studies and suggest that mechanical tension may also strongly influence neuronal behavior in vivo.

In the next step, efforts made to elucidate the key cytoskeletal components responsible for generating tension in axons (chapter 4). Towards this goal, a series of experiments were conducted on single axons of embryonic *drosophila* motor neurons in the presence of various drugs. To do this, each axon was slackened mechanically by bringing the neuro muscular junction (NMJ) towards the central nervous system (CNS) multiple times. In the absence of any drug, axons always shortened and restored the straight configuration each time within 2-4 minutes of slackening. The

total shortening was about 40% of the original length. The recovery rate in each cycle, but not the recovery magnitude, was dependent on the number of times the axon had previously been slackened. This recovery however was significantly hampered with the depletion of ATP, inhibition of myosin motors, and disruption of actin filaments, but not with the disruption of microtubules. These results suggest that the actomyosin-machinery is the major active element in axonal contraction while microtubules contribute passively and minimally.

In the last attempt, the diametric regulation of single axon of Drosophila neurons subject to external stretch and control (free or intact) was investigated. It was observed that normalized average diameter of stretched axons (subjected to 20-25% strain for 30 min) decreased vs to those in control experiments. Interestingly, the decrease in average diameter continued even after removing the external stretch at least for 25 minutes. This trend however was noticeably reversed by applying pharmaceutical drugs that inhibit motor proteins or disrupting cytoskeletal structure, both for free and stretched axons cases. The average diameter of free axons increased by inhibition of Myosin II or disrupting F-actin but reduced when microtubules were disrupted. Similar trend was also observed for stretched axons when they were treated with the same set of drugs.

As a continuation of current work, which can be developed in future yet with a slightly different direction, I would like to conclude this dissertation with two interesting work that have been initiated with preliminary results.

i) Local tracking of axon contraction. The contraction analysis previously discussed in chapter 4 considered the axon as a continues bulk system. The global contraction of axon were estimated based on the instantaneous change in total length of the axon while its end points were fixed. Although this analysis provided us with a the quantitative values for the extent and rate of axonal contraction at different slackening cycles, yet it is not sufficient to estimate the local strain of the axon. In short, the current analysis only provide an average value of axonal contraction , i.e. not local, due to lack of distinct markers along the axon membrane.

To relax this limitation, I developed a technique, using a high pressure syringe-type chamber, to deposit the fluorescent nano- particles (beads at ~ 200 nm diameter) onto the axon membrane in Drosophila embryos (Fig 6.1). These nanoparticles serve as a train of distinct and tractable marker during time lapse imaging of axons, in particular, when they are subjected to external

stretch or compression. Given that the size of nano-particles deposited on the axon membrane is 200 nm while axon diameter in micron range, this technique allows us to estimate local deformation of small segments along the axons (i.e. strain density function) with an admissible accuracy, both in compression and stretch.

Having calculated distributive contractile strain along the axon, we will be able to obtain a better idea whether axonal contraction is happening all along the length, or it is an end-pulling effect. The outcome of the analysis will also elucidate the intensity and direction of segmental deformation at various point of axon.

ii) Time lapse recording of neuronal development and synaptogenesis formation in live Drosophila embryo. In order to investigate and monitor the progression of axon growth (time rate and length) and formation of synapses and Neuro Muscle junction (NMJ) since the early stage to the larva stage, we used the Light-sheet microscope. The Light-sheet microscopy technically allows rapid, high-contrast, volumetric imaging of embryo for several hours with minimal sample fluorescent exposure.

A few images of progressive development of transgenic Drosophila embryos (inside the egg's shell, not-dissected) are shown in Fig 6.2. With continuing the use of Light-sheet imaging techniques in future ,we will have a clearer idea how embryonic *Drosophila* neurons develop spatially (3D visualization at various segments of the embryo) and temporally(over a long period of time lapse imaging) with minimum exposure time.

Figures

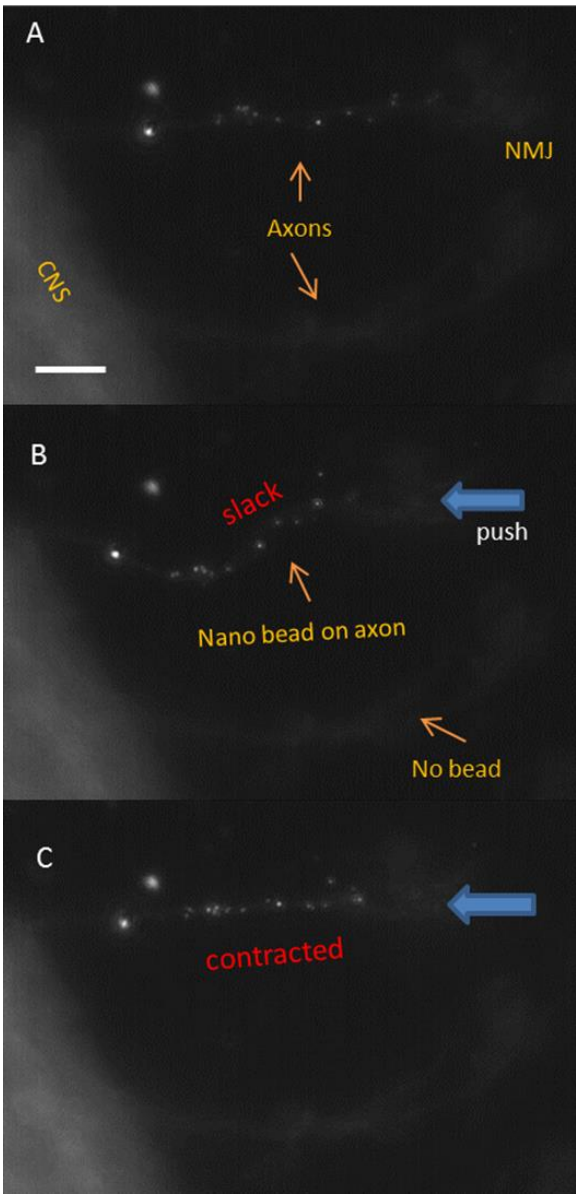

Figure 6.1 . A: The fluorescent nano- particle beads (200 nm in dia) deposited on axon membrane served as point-wise markers to facilitate optical tracking of axon deformation subjected to an external stimuli. B: The marked axon is being pushed from its Neuro Muscle junction (NMJ) with a microneedle (not shown) and became slack. C: Axon contracted within a few minutes after compression. Note that in all cases nano particles nicely follow the deformed configuration of axon, allowing to estimate distribution of local strain along the axon over time with a reasonable accuracy. Scale bar = 10 μm.

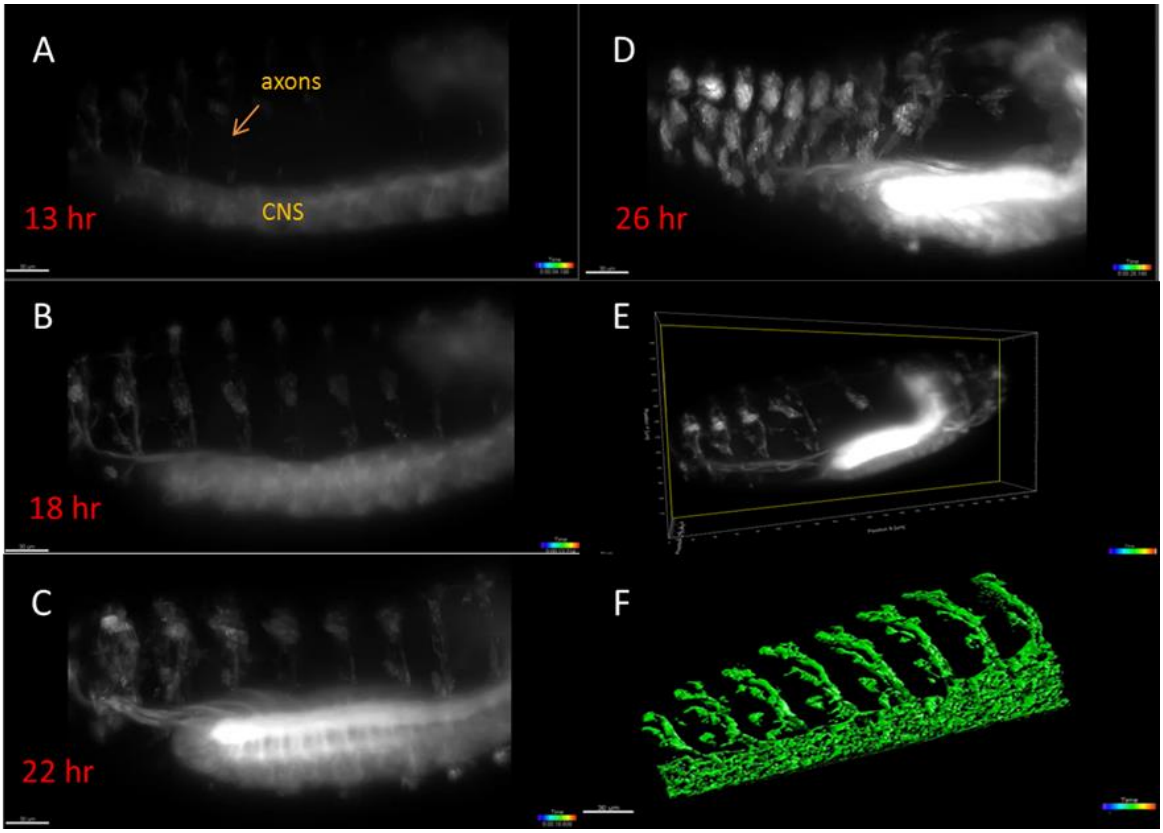

Figure 6.2: A-E: The florescent images obtained in Light-sheet microscope, progressively showing spatial and temporal axonal growth and shortening the CNS length inside the *Drosophila* embryo at different stages. F: fluorescent 3D stack images of embryo. Scale bar =30 μm.